Identifying the onset of the Messinian salinity crisis: a reassessment of the biochronostratigraphic tools (Piedmont Basin, NW Italy)

Francesca Lozar [1*], **Donata Violanti** [1], **Elisa Bernardi** [1], **Francesco Dela Pierre** [1], **Marcello Natalicchio** [2]

[1] Dipartimento di Scienze della Terra, Università degli Studi di Torino, Via Valperga Caluso, 35, 10125 Torino, Italy

[2] Institut für Geologie, Universität Hamburg, Bundestra β e 55, 20146 Hamburg, Germany

[*] Corresponding author; email: francesca.lozar@unito.it

Keywords. Calcareous nannofossils, foraminifers, Messinian salinity crisis, Mediterranean.

Running head: Biochronostratigraphic events at the onset of the Messinian Salinity crisis

Abstract

At the end of the Miocene, water exchange between the Mediterranean Sea and the world ocean was severely reduced, leading to deposition of huge volumes of evaporites during the Messinian salinity crisis (MSC). The onset of this event has been precisely dated at 5.971 Ma by means of magneto-, bio- and cyclostratigraphic tools, but clear paleobiological proxies for its recognition are so far missing, especially in those basins in which evaporite deposition is delayed. The disappearence of calcareous microfossils was the only paleobiological signal used to approximate the beginning of the crisis, but recently calcareous plankton has been recorded above the onset in several sections. Calcareous nannofossil and planktonic foraminifer data from the Piedmont Basin indicate that the cycle recording the beginning of the crisis is characterized by a peculiar succession

of bioevents. These bioevents are (i) a calcareous nannofossil *Sphenolithus abies* abundance peak, followed or accompanied by minor peaks of *Helicosphaera carteri*, *Umbilicosphara rotula* and *Rhabdosphaera procera*, and (ii) the planktonic foraminifer *Globorotalia scitula* and *G. suterae* influx. The same sequence of bioevents has been recorded in sections from the Eastern and Central Mediterranean (Pissouri and Tokhni sections in Cyprus; Fanantello section in the Apennines) within the same age range. We thus propose that the *S. abies* and *U. rotula* peaks (often accompanied by minor peaks of *H. carteri* and *R. procera)* provide a reliable tool for the identification of the onset of the MSC independently from the occurrence of evaporites. This is particularly useful when studying successions deposited in intermediate- and deep-water basins, where evaporites are absent or their deposition is delayed. Our findings can potentially provide a reliable proxy for the identification of the MSC onset in deep-sea cores.

1. Introduction

The Messinian Salinity Crisis was a dramatic palaeoceanographic event driven by the combined effects of climatic and geodynamic factors that controlled the connections between the Mediterranean Sea and the Atlantic Ocean (and possibly with the fresh water Paratethyan basins) (Roveri et al. 2014, Flecker et al. 2015, and references therein). The reduced water exchange between the basins was held responsible for the deposition of huge volumes of evaporites (carbonates, gypsum and halite) and brackish water sediments, which accumulated through three evolutionary stages (Roveri et al. 2014). The chronostratigraphic framework of the three main stages characterizing the onset, development and termination of the MSC has been achieved integrating different stratigraphic tools such as biostratigraphy, magnetostratigraphy, isotope stratigraphy and cyclostratigraphy (Roveri et al. 2014, and references therein). Stage 1 (5.97-5.60 Ma) was characterized by the synchronous deposition of primary sulphate evaporites in peripheral basins (the Primary Lower Gypsum unit, hereafter termed PLG unit; Roveri et al. 2008) and gypsum-free euxinic shale in the deep basins (Manzi et al. 2007, CIESM 2008, Roveri et al. 2014).

During Stage 2 (5.60-5.55 Ma), the marginal basins underwent subaerial exposure and erosion as evidenced by an erosional surface referred to as Messinian erosional surface (MES); this surface can be traced basinward as a correlative conformity at the base of thick accumulations of chaotic and resedimented evaporites (the Resedimented Lower Gypsum unit, hereafter termed RLG unit; Roveri et al. 2008) sourced by the dismantling of the PLG unit (Roveri et al. 2003, Manzi et al. 2005). Thick halite bodies were also deposited during this stage. Stage 3 (5.55-5.33 Ma) was characterized by deposition of a new unit of sulphate evaporites (Upper Evaporites) in the SE sectors of the Mediterranean (Sicily, Ionian Islands, Crete, and Cyprus), and by clastic deposits in the Western and Northern basins (Spain, Northern Apennines, Piedmont Basin). The re-establishment of fully marine conditions at 5.33 Ma (Lourens et al. 2004), leading to the deposition of Zanclean marine sediments, marks the end of the salinity crisis.

Regarding the first stage of the MSC, recent work suggests that in intermediate- to deep-water settings (*sensu* Roveri et al. 2014) gypsum deposition did not begin synchronously with the margins, but was instead delayed by tens of thousands of years (Manzi et al. 2007, Dela Pierre et al. 2011, Gennari et al. 2013, Manzi et al. 2013, Violanti et al. 2013). As a consequence, the identification of the MSC onset is less easily accomplished in intermediate- to deep-water settings compared to marginal settings, where this event coincides with the base of the PLG unit.

The Piedmont Basin, the northernmost offshoot of the Mediterranean Sea (Fig. 1A), is an ideal site to identify the exact position of the MSC onset in deeper-water environments where gypsum is absent or its deposition is delayed. In fact, the Piedmont Basin preserves sedimentary successions of both marginal and intermediate-water depositional environments that can be correlated through the integration of bio- and cyclostratigraphic studies (Fig 1B; Dela Pierre et al. 2011, Violanti et al. 2013).

Based on detailed micropalaeontological analyses of the calcareous microfossil assemblages, this study aims at providing a reliable biostratigraphic tool to identify the onset of the MSC in intermediate-water depositional environments where this event is not marked by significant

lithological changes (e.g., appearance of sulphate evaporites) and to test its reliability for stratigraphic correlations at a Mediterranean-Basin-wide scale.

2. Geological setting of Messinian salinity crisis deposits in the Piedmont Basin

The evolutionary stages of the Messinian salinity crisis are recorded in the Piedmont Basin by the following lithostratigraphic units: the Sant'Agata Fossili Marls (SAF: pre-MSC and MSC Stage 1 p.p.), Primary Lower Gypsum unit (PLG; MSC Stage 1), Valle Versa Chaotic Complex (VVC; MSC Stage 2), and the Cassano Spinola Conglomerates (CSC; MSC Stage 3) (Fig. 1B; Dela Pierre et al. 2011). The upper part of the SAF consists of shale/marl cycles, each few metres thick, directly followed by shale/gypsum cycles of the PLG unit. At the southern margin of the Piedmont Basin (Arnulfi section; Dela Pierre et al. 2011), the SAF are overlaid by the first shale/gypsum cycle of the PLG unit, but towards the deeper part of the basin (Pollenzo section; Dela Pierre et al. 2011, Violanti et al. 2013) the basal gypsum cycles are replaced by correlative shale/marl cycles still belonging to the SAF (Fig. 1B). In the Piedmont Basin, the stacking pattern of the gypsum facies of the PLG unit (Dela Pierre et al. 2011, 2012) matches that described for the Mediterranean Basin (Lugli et al. 2010). A remarkable facies change is observed from the sixth PLG cycle upwards, marked by the appearance of the branching selenite facies. The gypsum bed belonging to the sixth PLG cycle is a distinct marker bed termed the Sturani Key Bed (SKB, Dela Pierre et al. 2011). It can be traced laterally over the entire basin, providing a reliable physical stratigraphic correlation horizon (Fig. 1B). The PLG unit is truncated at the top by an erosional surface corresponding to the Messinian Erosional Surface (MES) (Fig. 1B; Dela Pierre et al. 2011). Above the MES, the chaotic sediments of the Valle Versa Chaotic Complex (MSC Stage 2) and the Cassano Spinola Conglomerate (MSC Stage 3) crop out and are finally topped by deep-water Zanclean marls (Argille Azzurre Fm.; Violanti et al. 2009) recording the re-establishment of fully marine conditions at the end of the MSC (Fig. 1B).

3. Material and methods

This work is based on stratigraphic and micropalaeontological data from the Banengo and Moncalvo sections, cropping out on the northern margin of the Piedmont Basin, and new micropalaeontological data from the Pollenzo section (southern margin of the PB) which has been previously studied by Lozar et al. (2010), Dela Pierre et al. (2011) and Violanti et al. (2013) (Fig. 1). The examined sections preserve the boundary between the SAF and the primary evaporites of the PLG unit. The Pollenzo section has been selected for its straightforward correlation to the Mediterranean reference sections cropping out in the Eastern, Western and Central Mediterranean (Pissouri, Abad, and Falconara; Krijgsman et al. 1999, Sierro et al. 2001, Blanc-Valleron et al. 2002).

3.1. Studied sections

3.1.1. Banengo

The Banengo section (Figs. 2-4) is located in the Saint Gobain gypsum quarry close to the village of Montiglio. It consists of a huge block belonging to the Valle Versa chaotic complex: in this block, however, the upper part of the SAF and four cycles of the PLG unit are preserved.

The upper part of the SAF is composed of five lithologic cycles consisting of laminated shale and massive marl couplets (Bm1-Bm5). Sediments belonging to the Bm5 cycle contain abundant siliceous sponge spicules. Decimetre to metre-thick biocalcarenite beds masking the “normal” sedimentary pattern occur in these cycles. The SAF is overlaid conformably by four shale/gypsum cycles (Bg1-Bg4) belonging to the PLG unit. The gypsum beds of the lower three PLG cycles consist of massive selenite. The fourth cycle is characterized by massive selenite grading upwards to banded selenite. The shale semicouplets of the PLG cycles are up to 3 m thick. They show a lamination defined by the alternation of clay and carbonate-rich laminae.

3.1.2. Moncalvo

129 The Moncalvo composite section (Figs. 5-7) integrates core and outcrop data from the gypsum
130 quarry located in the small town of Moncalvo and owned by Fassa Bortolo s.r.l.
131 A drillcore comprising the stratigraphic boundary between the SAF and the PLG unit was studied
132 for this work. The lower five metres belong to the uppermost part of the SAF and consist of four
133 lithologic cycles. The elementary cycle is made up of grey laminated shales and light grey massive-
134 homogeneous marls (cycles Mm1-Mm4). In Cycle Mm1, the laminated shales are replaced by silty
135 marls. The upper part of the core comprises the lower PLG cycle (Mg1) which consists of a 1-m-
136 thick grey muddy layer rich in millimetre to centimetre-sized lenticular gypsum crystals overlaid by
137 a massive selenite bed (Bernardi 2013). The overlying four cycles are exposed in the Moncalvo
138 quarry (Mg2-Mg5). The gypsum beds of the lower three PLG cycles (Mg1 to Mg3) consist of
139 massive selenite, whereas Cycle Mg4 is composed of the branching selenite facies, which also
140 typifies Cycle Mg5. Thickness and facies of Cycle Mg4 strictly resemble those of the Sturani Key
141 Bed recognized in the Alba region (Pollenzo and Arnulfi sections), where it represents the sixth
142 PLG cycle (Dela Pierre et al. 2011).
143 3.1.3. Pollenzo
144 The Pollenzo section (Figs. 8-10) crops out on the left bank of the Tanaro River; it consists of seven
145 shale/marl cycles (and interbedded carbonate-rich layers) of the SAF (Pm1-Pm7), overlaid by
146 shale/gypsum cycles of the PLG unit (see Dela Pierre et al. 2011, 2012 for details). The section has
147 been recently studied by means of physical stratigraphy, micropalaeontology, magnetostratigraphy,
148 and stable-isotope geochemistry (Lozar et al. 2010, Dela Pierre et al. 2011, 2012, Violanti et al.
149 2013). It has become a reference section for the northernmost part of the Mediterranean basin since
150 its record has been correlated to the reference sections of the western and central Mediterranean
151 (Violanti et al. 2013).
152
153 3.2. Micropalaeontological analyses

Thirty-one samples from the Banengo section and twenty-three samples from the Moncalvo sections were studied. Results obtained from fourty-three samples from the Pollenzo section were published in previous works (Lozar et al. 2010, Violanti et al. 2013). For the present study unpublished data on selected calcareous nannofossil species and on planktonic and benthic foraminifers were added.

3.2.1. Calcareous nannofossils

Standard smear-slides were prepared for each sample and observed at 1250X in polarized light. For quantitative analysis, a total of 500 specimens were counted from each sample. In the studied samples, calcareous nannofossils (CN) are well to moderately preserved. In the Banengo and Pollenzo samples, CN were abundant to common, whereas the group showed a lower abundance in the Moncalvo samples. Abundances of very rare selected taxa (*Discoaster* spp., *Amaurolithus* spp.) were determined by counting 4.5 mm^2 on each slide. We included *Reticulofenestra minuta* and *R. haqii* in the informal group of small *Reticulofenestra* (Pujos 1987, Flores et al. 2005).

3.2.2. Foraminifers

About 150 g of dry sediment were soaked with water and a small amount of hydrogen peroxide, washed, sieved into fractions (greater than 250 μm, 125–250 μm and 63–125 μm), dried and weighed. The three fractions were examined separately. Taxonomic determination of foraminiferal species followed Kennett and Srinivasan (1983) for planktonic taxa, Van Morkhoven et al. (1986), Loeblich and Tappan (1988), Sgarrella and Moncharmont Zei (1993) and Milker and Schmiedl (2012) for benthic species. Quantitative analyses were carried out on the total >125 μm residues, splitted in fractions yielding about 300 specimens.

For each sample, percentages of planktonic and benthic taxa were calculated relative to the sum of the total planktonic and benthic specimens, respectively. The P/(P+B) ratio was also calculated, as P/(P+B)*100, where P and B represent the total number of planktonic and benthic foraminifers, respectively. The benthic diversity was measured using the Shannon Index (H), using PAST ver. 1.77 (Hammer et al. 2008). Following Bé and Tolderlund (1971), Hemleben et al. (1989), Pujol and

Vergnaud Grazzini (1995) and Serrano et al. (1999) for planktonic taxa and Wright (1978), Sgarrella and Moncharmont Zei (1993), Kouwenhoven et al. (1999), Murray (2006), and Alve et al. (2016) for benthic taxa, palaeoenvironmental indices were established. These are: 1) the percentages of planktonic warm-water oligotrophic indicators (W/O) (*Globigerinoides* spp. including *G. bulloideus, G. obliquus, G. ruber,* and *G. trilobus*, *Globoturborotalita* gr. including *Gbt. apertura, Gbt. decoraperta, Gbt. woodi*, and *Orbulina* spp. including *Orbulina universa* and the morphotype *O. suturalis*) (Hemleben et al. 1989, Serrano et al. 1999); 2) the percentages of cool-water eutrophic indicators (C/E) (*Globigerina bulloides, G. falconensis,* Neogloboquadrinids, *Globorotalia scitula* gr., and *Turborotalita quinqueloba*); 3) the percentages of deep outer neritic to bathyal benthic taxa (DO/B) (*Bulimina aculeata, B. minima*, *Cassidulina* spp., *Cibicidoides* spp., *Globobulimina* spp., *Globocassidulina* spp., *Gyroidinoides* spp., *Heterolepa* spp., *Melonis* spp., *Planulina ariminensis, Pullenia* spp., *Sphaeroidina bulloides,* and *Uvigerina* spp.; a full list of DO/B taxa is given in Appendix 1); 4) the percentages of inner neritic shallow-water (SW) benthic taxa *(Ammonia* spp., *Cibicides lobatulus, Discorbis* spp., *Elphidium* spp., *Glabratella* sp., *Neoconorbina* spp., and *Rosalina* spp.; a full list of SW taxa is given in Appendix 2). *Bolivina dentellata, B. arta, B. pseudoplicata, Brizalina dilatata,* and *B. spathulata* are grouped in *Bolivina* spp.

4. Results

4.1. Banengo

Qualitative analyses of foraminiferal assemblages were carried out on twenty-seven samples, since the four uppermost samples were barren of calcareous microfossils. Ten of the studied samples contained extremely scarce and badly preserved planktonic foraminifers and were useful only for quantitative analysis of their benthic assemblage (samples 2.30 m – base of Cycle Bm2; 3.60 m in

205 Cycle Bm2; 7.45, 7.65, 8.20, 8.85 m in Cycle Bm4; 9.05, 9.40, 10.20, 10.85 m in Cycle Bm5). The
206 two uppermost samples (11.73 and 11.93 m) yielded only fish debris and sponge spicules.
207 The preservation of calcareous microfossil was moderate to poor in most of the samples . Besides
208 foraminifers, ostracods, bivalves and vegetal frustules were also recovered in the residues. Many
209 samples in the interval between 9.0-12.55 m (Cycles Bm5 and Bg1) yielded common to very
210 abundant siliceous sponge spicules (mainly megascleres) and bryozoan fragments (work in
211 progress).
212 4.1.1. Calcareous nannofossils
213 Calcareous nannofossil assemblages are dominated by small placoliths, such as *Reticulofenestra*
214 *minuta* and *R. haqii* (small *Reticulofenestra* in Flores et al. 2005), accounting for up to 80% of the
215 total assemblage. *Coccolithus pelagicus* and *Calcidiscus leptoporus* are fairly abundant and account
216 for up to 10-15% of the total assemblage; abundant *Sphenolithus abies*, *Helicosphaera carteri*,
217 *Umbilicosphaera rotula*, *Rhabdosphaera procera*, and *U. jafari* are recorded in discrete intervals
218 (Fig. 2). *Discoaster* spp. are scarce or absent. *Amaurolithus delicatus* is present only in the basal
219 samples. Small placoliths, mainly belonging to the genus *Reticulofenestra*, show abundances from
220 40 to 80% from the bottom of the section to 8.85m (base of Cycle Bm5); above this level, their
221 abundance drops to 40% or less. In general, specimens of the *Reticulofenestra* lineage are very
222 common and most abundant in the upper marls of each cycle (Fig. 2). Abundances of *Cd.*
223 *leptoporus* increase from the bottom to the top of each cycle from the base of the section up to 8.85
224 m (base of Cycle Bm5), where they drop to 0%. The highest abundances were recorded in the marly
225 layers (up to 8%); they covary with the abundance trend of small *Reticulofenestra*. *Sphenolithus*
226 *abies* is relatively abundant (up to 20%) in the shaly bed of each cycle. A remarkable high
227 abundance peak (up to 60%) was recorded at 9.05 m in the shale of Cycle Bm5 (Fig. 2).
228 *Helicosphaera carteri* and *U. rotula* abundances are lower than 10% up to 8.85 m, but reach
229 respectively 30% and 20% in Cycle Bm5. *Rhabdosphaera procera* abundance is low along the
230 entire section, but reaches 20% at the top of the shale in Cycles Bm1 and Bm5. *Umbilicosphaera*

231 *jafari* is fairly abundant in the middle part of the section, were it account for up to 40% of the total
232 assemblage.
233 4.1.2. Foraminifers
234 Planktonic foraminifers are common to dominant in the shales and massive marls of Cycles Bm1
235 and Bm3, very scarce upwards (10 to 20%; Fig. 3). In general, the W/O group is dominant in the
236 shale of Cycles Bm1, Bm2, Bm3, and Bm5. The C/E taxa are abundant in the marls (Cycles Bm1,
237 Bm3) but also in the shale of Cycle Bm5. Among the W/O taxa, the genus *Orbulina* (Hemleben et
238 al. 1989) is frequent to common in Cycles Bm1 to Bm3, very rare or absent in the overlying
239 samples. *Globigerinoides* spp. and *Globoturborotalita* spp. are absent or rare, but show an
240 abundance peak at 10.20 m (13.45%), and 10.60 m (50%), respectively. Among the C/E taxa *G.*
241 *bulloides* (Hemleben et al. 1989) is rare. *Neogloboquadrina acostaensis* occurs in the shale of each
242 cycle; left-coiled tests are dominant in most samples, whereas right-coiled forms are dominant in
243 Cycles Bm3 and Bm5. *Turborotalita quinqueloba* is the most abundant C/E species (up to 70 % in
244 Cycles Bm1 and Bm3),. *Turborotalita multiloba* is common in Cycle Bm1, but also occurs in Cycle
245 Bm3, with very small tests. Two *G. scitula* and *G. suterae* influxes were recognized at the top of
246 Cycle Bm2 and in the shales of Cycle Bm5.
247 Benthic foraminifers are common to abundant and show low to medium species diversity. *Bolivina*
248 spp. and *Bulimina echinata*, infaunal stress-tolerant taxa (Violanti 1996, Barbieri and Panieri 2004,
249 Van Hinsbergen et al. 2005, Murray 2006, Diz and Frances 2008), are frequent (Fig. 4). *Hanzawaia*
250 *boueana* and *Valvulineria bradyana* (epifaunal shelf species; Bergamin et al. 1999, Murray 2006)
251 occur in Cycles Bm1 to Bm4. In Cycles Bm1 to Bm4 abundances of DO/B species are around 20-
252 30% and drop upwards to (0-4%). Shallow-water taxa are abundant, particularly in Cycles Bm2 and
253 Bm3.
254 The diversity of benthic foraminiferal assemblages shows rather small fluctuations throughout the
255 succession, and the Shannon Index (H) ranges between 1.05 (sample 14.4 m) and 2.54 (sample 8.05
256 m).

257 Very rare and poorly preserved specimens of *Bolivina* spp, *B. echinata* and *Globocassidulina*
258 *subglobosa* occur in the >125 μm and 63-125 μm fractions of sample 11.60 m (cycle Bg1).
259
260 4.2. Moncalvo
261 The uppermost ten samples were devoid of calcareous microfossils, but yielded siliceous
262 microfossils; the topmost three samples were barren. Foraminiferal quantitative analyses were
263 carried out on nine samples. The lowermost two samples yielded extremely rare specimens,
264 whereas samples at 132.00 m and at 130.90 m (Cycles Mm1 and Mm3, respectively) were barren of
265 foraminifers (Fig. 6, 7).
266 Common to abundant diatoms were detected in the smear slides, being abundant in the laminated
267 shale to very rare or absent in the homogeneous marls, and showing higher abundances in the shales
268 of the lower part of Cycle Mm3 and of Cycle Mm4 (Fig. 5).
269 The washing residues were dominated by the inorganic material (microcrystalline whitish
270 aggregates, gypsum crystals and mica flakes). Within the biogenic fraction of the washing residues,
271 poorly preserved radiolarians were common at 130.60 m (laminated shale of cycle Mm3). Siliceous
272 sponge spicules and demosponge microscleres were very abundant in the upper part of Cycle Mm2
273 and in the lower part of Cycle Mm3 as well as bryozoan fragments (work in progress). Mollusk and
274 echinoid fragments seldom occurred, fish debris (otoliths, scales, teeth, vertebrae) and vegetal
275 frustules were common to abundant. In the uppermost samples only siliceous microfossils (diatoms,
276 sponge spicules), fish and vegetal debris were recorded.
277 4.2.1. Calcareous nannofossils
278 In this section calcareous nannofossil abundance is generally less than 500 individuals per mm^2
279 except for few peaks of 500 and 1 500 individuals per mm^2 (Fig. 5). Calcareous nannofossil
280 assemblages are dominated by small *Reticulofenestra* (*R. minuta* and *R. haqii*), reaching up to 70%
281 of the total assemblage and slightly increasing towards the top (Fig. 5). Minor components of the
282 assemblage are *C. pelagicus, Reticulofenestra antarctica*, *S. abies*, *H. carteri*, *U. rotula*, *R. procera*,

283 and *U. jafari*. *Umbilicosphaera rotula*, when present, is very abundant and shows an opposite
284 pattern with respect to *R. minuta. Discoaster* spp. are very rare and *Amaurolithus* spp. are absent
285 from the studied material, possibly due to the proximal location of the section with respect to the
286 northern margin of the Piedmont Basin. *Coccolithus pelagicus* and *R. antarctica* never exceed 12%
287 of the assemblage, displaying an opposite distribution pattern; *R. antarctica* shows higer
288 abundances in the marly beds of each cycle. *Sphenolithus abies* shows abundances lower than 5% in
289 all samples except for a peak at 130.70 m (Cycle Mm3). *Helicosphaera carteri* shows fluctuating
290 abundances, never exceeding 8%. *Umbilicosphaera rotula* shows two prominent peaks at 132.80
291 and 131.80 m (Cycle Mm1), and a minor peak at 130.70 m. *Rhabdosphaera procera* reaches 1% at
292 130.70 m, i.e., in the same sample recording the *S. abies* peak. *Umbilicosphaera jafari* is always
293 very rare, except for a peak at 130.90 m in Cycle Mm3.
294 4.2.2. Foraminifers
295 Countings of the >125 μm planktonic and benthic foraminifers were carried out on seven samples,
296 disregarding the very poor or barren residues at 133.00, 132.80, and 132.00 m (Cycle Mm1), 130.90
297 m (Cycle Mm2), 130.45 m and 130.30 m (Cycle Mm3). Species diversity is often low, and
298 preservation is often poor. Rare specimens of the planktonic *T. quinqueloba* occur in the 63-125 μm
299 fraction of samples 130.45 m and 130.30 m (Cycle Mm3; Fig. 6, 7); very rare juvenile benthic
300 forms (*Cibicidoides* sp.) were detected in sample 130.45 m.
301 The P/(P+B) ratio displays its highest value in the silty marls of Cycle Mm1 (65.74%, 132.30 m).
302 Planktonic specimens are rare in the laminated shales. Among the planktonic W/O taxa, *Orbulina.*
303 spp. are scarce in the lowermost Mm1 Cycle and rather frequent only in the shales of Cycle Mm2
304 (Fig. 6). *Globigerinoides* spp. (mainly *G. obliquus*) represent about 10% of the assemblage in Cycle
305 Mm1, but also occur in the marls of Cycle Mm2 in lower abundances. *Globoturborotalita* spp.
306 show a similar pattern with higher abundances (up to 40%). The cool-water cutrophic *G. bulloides*
307 is common to frequent in the marls, together with *N. acostaensis*, *T. quinqueloba* and scarcer
308 *Globigerinita* spp. *Neogloboquadrina acostaensis* is dominantly dextral coiled, but shows a coiling

309 change in the shales of Cycle Mm2. *Turborotalita multiloba* occurs in very low percentages and
310 with small-sized tests in the marls of Cycle Mm2. Small specimens of *G. scitula* and *G. suterae*
311 show an abundance peak at 130.70 m (Mm3 shales). The W/O taxa are abundant in the shales of
312 Cycles Mm1 and Mm2, and progressively decrease and ultimately disappear in Cycle Mm3. The
313 C/E planktonic species show a nearly opposite pattern.
314 Benthic foraminifers are common to very frequent, but exhibit a low diversity. Stress-tolerant
315 infaunal forms (Violanti 1996, Van Hinsbergen et al. 2005, Murray 2006), represented by *Bolivina*
316 spp. and *B. echinata* are the dominant taxa (Fig. 7). Shelf epifaunal taxa, such as *H. boueana* and *V.*
317 *bradyana* are less common or very rare, respectively. Deep outer neritic to bathyal benthic taxa
318 (Fig. 7) are dominant only at 132.30 m (Cycle Mm1). In the upper samples, the benthic assemblage
319 is almost completely represented by shallow-water epiphytic taxa.
320 The Shannon Index (H) of benthic diversity reaches highest values (2.89) at 132.30 m in Cycle
321 Mm1 and decreases upwards, to a minimum value of 0.69 at 130.30 m.
322
323 4.3. Pollenzo
324 In the studied samples the preservation of calcareous microfossils is generally good. In the washing
325 residues, besides foraminifers, ostracods and bivalve fragments are very rare; fish and vegetal
326 debris are common in the upper samples.
327 4.3.1. Calcareous nannofossils
328 Calcareous nannofossil assemblages have already been discussed in previous studies (Lozar et al.
329 2010, Violanti et al. 2013). Main results, useful for the present discussion, were the high abundance
330 of *R. minuta* across the seven cycles of the SAF (Pm1-7), the increasing abundance of *C. pelagicus*,
331 and the higher abundance of *Discoaster variabilis* gr. in the shale of each cycle, that overall
332 negatively correlates with the abundance of *C. pelagicus*. This cyclicity was demonstrated to be
333 driven, as in other Mediterranean sections (e.g., Flores et al. 2005), by precessional forcing (Dela
334 Pierre et al. 2011, Violanti et al. 2013). The base of Cycle Pm5 is characterized by an abundance

335 peak of *S. abies* (62%) together with a peak of *H. carteri* (22%), followed by another *H. carteri*
336 peak (27%) together with *R. procera* (13%); in contrast, the abundances of these species are low (5
337 to 10%) in the lower cycles. A new sample from the limestone bed *e* at the top of Cycle Pm5 (Fig.
338 8) yielded an oligospecific assemblage consisting of *U. rotula* (65%) and small *Reticulofenestra*
339 (Fig. 8). Above Cycle Pm5, the section is characterized by lower abundances of calcareous
340 nannofossils and by oligospecific assemblages often dominated by small *Reticulofenestra* and *U.*
341 *jafari*; the latter taxon is also abundant in cycles Pm1 and Pm2.
342
343 4.3.2. Foraminifers
344 New information is presented here integrating the data reported in a previous study (Violanti et al.
345 2013) . The P/(P+B) ratio is high in the shale of each cycle and in the marls of Cycle Pm5 (Violanti
346 et al. 2013). Among the W/O taxa, *Orbulina* spp. is abundant in Cycles Pm1, Pm3 and Pm4. Rare
347 *Globigerinoides* spp. (mainly *G. obliquus*) and rather common *Globoturborotalita* spp. occur only
348 in the shale of Cycles Pm1 and Pm2. The C/E phytophagous *Globigerinita* spp. is common in the
349 laminated shales, but also occurs in the marls of Cycles Pm1 and Pm5. The planktonic assemblage
350 in the homogeneous marls is absent or very scarce, poorly diversified, and represented by C/E taxa.
351 *Globigerina bulloides* is frequent within the topmost marl and lower shales of Cycles Pm1 and Pm2
352 and in the Pm3 marls. The taxon is common, together with *G. glutinata* and *T. quinqueloba*, at the
353 top of the Pm5 marls. *Neogloboquadrina acostaensis* is dominantly dextral coiled in Cycles Pm1,
354 Pm3, and Pm4; sinistral coiled tests are dominant in Cycles Pm2 and Pm5. *Turborotalita multiloba*
355 occurs only in Cycle Pm1. *Globorotalia scitula* and *G. suterae*, represented by small specimens,
356 occur in the laminated shales of Cycle Pm2 and in the upper part of Cycle Pm5. The new data show
357 the strong dominance of C/E taxa in most of the succession (Fig. 9). The W/O species are restricted
358 to the laminated shales (Fig. 9) and are dominant only in Cycle Pm1
359 At Pollenzo, benthic foraminifers are absent or very rare in the laminated shales, whereas they are
360 dominant in the marly layers (Fig. 10). *Bolivina* spp. and *B. echinata* are the most abundant taxa.

361 Shelf epifaunal taxa are abundant in Cycles Pm3 and Pm6 (*H. boueana*) and in Cycles Pm1 and
362 Pm4 (*V. bradyana*). DO/B benthic taxa (Fig. 10) show one frequency peak in Cycle Pm5. In the
363 other samples the DO/B values rarely exceed 10% of the benthic assemblage. SW taxa (Fig. 10) are
364 the only benthic foraminifers in most of the laminated shales.
365 The benthic diversity, as expressed by the Shannon Index (H) is highest in the lower samples and
366 progressively decreases upwards.
367 Small sized foraminifers (63-125 μm and <63 μm) occur up to Cycle Pm7, where both planktonic
368 and benthic taxa disappear (Violanti et al. 2013).
369

370 **5. Discussion**

371 5.1. Calcareous plankton biostratigraphy

372 The scattered, but continuous occurrence of the calcareous nannofossil *A. delicatus* in the Banengo
373 section allows the correlation to the Messinian MNN11b/c Zone (Raffi et al. 2003); this marker was
374 not recorded in the Moncalvo section, where the micropalaeontological record is dominated by high
375 abundance of diatom frustules, indicating high nutrient availability in the upper water column.
376 *Amaurolithus delicatus* is an open ocean taxon rare in Mediterranean sections (Raffi et al. 2003),
377 probably favoring meso- to oligotrophic waters; the proximity to the shore and the high nutrient
378 loading suggested by the common occurrence of diatom frustules may have limited or inhibited its
379 occurrence in the water column.
380 Foraminiferal assemblages of the SAF cropping out in the Banengo and Moncalvo sections can be
381 referred to the Messinian interval Subzone MMi13c (Lourens et al. 2004) and the *T. multiloba*
382 subzone (D'Onofrio et al. 1975), on the basis of the presence of *T. multiloba*, whose FCO was dated
383 at 6.42 Ma (Lourens et al. 2004, Iaccarino et al. 2008); this bioevent defines the lower boundary of
384 the MMi13c subzone. This subzone is also characterized by the strong impoverishment of
385 foraminiferal assemblages, dominated almost exclusively by stress-tolerant planktonic and benthic
386 taxa. Subzone MMi13c has also been recognized in the Pollenzo section (Lozar et al. 2010, Dela

387 Pierre et al. 2011, 2012, Violanti et al. 2013). The upper part of the succession (Moncalvo cycles
388 Mm3 top and Mm4 and Banengo cycle Bg1) is barren of foraminifers and is referable to the Non-
389 distinctive Zone (NDZ, Iaccarino 1985).
390 The correlation among the Banengo, Moncalvo and Pollenzo sections is supported by the following
391 sequence of bioevents (in stratigraphical order):
392 1. the prominent *S. abies* peak, followed by *H. carteri*, *R. procera* and *Umbilicosphaera* spp.
393 peaks, recorded in Cycles Bm5 (Banengo) and Mm3 (Moncalvo) and already recognized in
394 Cycle Pm5 in Pollenzo (Lozar et al. 2010, Violanti et al. 2013) (Figs. 2, 5, 8);
395 2. the *G. scitula* and *G. suterae* influx recognized in the shale of Cycle Bm5 (Banengo), and in
396 Cycles Mm3 and Pm5 (Moncalvo and Pollenzo, respectively). In the three sections this
397 influx is positively correlated to a peak of cool-water eutrophic taxa (Figs. 3, 6, 9).
398 A secondary correlation tool at the Piedmont Basin scale is the last *Orbulina* spp. peak in the shale
399 of Cycle Bm3 (Banengo), Mm2 (Moncalvo), and Pm4 (Pollenzo), shortly preceding the *S. abies*
400 peak. In both the Banengo and Moncalvo sections this peak is followed by a short influx of *T.*
401 *multiloba* (>125 μm).
402 The correlation of the studied sections to the Mediterranean reference sections (Krjigsmann et al.
403 1999) is supported by the highest common occurrence (HCO) of *T. multiloba* (>125 μm) recorded
404 at 108 m in Pollenzo (Cycle Pm1) and at 1.7 m in Banengo (Cycle Bm1) (Fig. 11). Cycle Pm1 was
405 previously correlated to the UA31 cycle of the Abad composite section (Violanti et al. 2013), in
406 which a last small peak of *T. multiloba* was recorded in the fraction >150 μm (Sierro et al. 2001,
407 2003). The correlation to the Abad UA31 cycle is therefore extended to the Bm1 cycle of Banengo.
408 The HCO of *T. multiloba* was also recorded in Cycle 45 in the Falconara-Gibliscemi section in
409 Sicily (Hilgen and Krijgsman 1999, Blanc-Valleron et al. 2002) and in Cyprus (Krijgsman et al.
410 2002, Kouwenhoven et al. 2006, Orszag-Sperber et al. 2009, Gennari et al. this volume, where this
411 bioevent is numbered as 18a), thus allowing correlation to eastern Mediterranean sections. The
412 bioevent was assigned an age range of 6.04 - 6.08 Ma (Sierro et al. 2001).

413 The record of small *T. multiloba* in cycle Bm3 (Banengo) and Mm2 (Moncalvo) suggests that
414 locally this eutrophic planktonic taxon survived longer than previously recorded in the southern
415 Mediterranean successions of Spain (Sierro et al. 2001, 2003, Flores et al. 2005), Sicily (Di Grande
416 and Romeo 1980, Suc et al. 1995; Sprovieri et al. 1996, Blanc-Valleron et al. 2002), Greece
417 (Kouwenhoven et al. 2006), Cyprus (Orszag-Sperber et al. 2009), and central Italy (Iaccarino et al.
418 2008, Riforgiato et al. 2008, Gennari et al. 2013). Very low percentages of *T. multiloba* were
419 already recorded in Pollenzo in the 63-125 μm fractions (cycles Pm2 and Pm3; Violanti et al.
420 2013). We thus suggest that the last influx of small *T. multiloba* in the Banengo and Moncalvo
421 sections could be interpreted as the Last Local Occurrence (LLO) of this taxon in a particularly
422 favorable palaeoenvironment, with an age of about 6.0 Ma. The LLO of *T. multiloba* could be
423 proposed as a biostratigraphic event at the local scale, to be verified by further studies.
424
425 5.2. Cyclostratigraphy and identification of the MSC onset
426 In the Moncalvo section a well-defined cyclic lithologic stacking pattern made up of shale/marl
427 couplets characterizes the SAF. The relative abundance fluctuation of cool-well mixed water and
428 warm/stratified water taxa is in phase with the lithologic cyclicity. *Sphenolithus abies* (warm,
429 stratified waters; Perch Nielsen 1985, Gibbs et al. 2004) is more abundant in the shales, together
430 with the planktonic warm water foraminifers *Orbulina* spp. (Kennett and Srinivasan 1983,
431 Hemleben et al. 1989), and *Bolivina* spp. and *Brizalina* spp. (benthic infaunal, tolerating low
432 oxygen content and/or high organic matter fluxes to the sea floor) (Murray 2006, Alve et al. 2016).
433 In contrast, the marls of each cycle record higher abundances of *H. carteri* (mesotrophic waters;
434 Ziveri et al. 2000) and of C/E planktonic foraminifer taxa (Neogloboquadrinids and *Turborotalita*
435 spp.) (Kennett and Srinivasan 1983, Hemleben et al. 1989). The qualitative record of diatoms also
436 changes with lithology, from abundant in the shales to very rare or absent in the marls. High
437 nutrients input from the continent, possibly driven by high continental runoff, likely promoted the
438 high abundance of diatoms in the shale of each cycle. The high productivity of siliceous plankton

439 could also justify the low abundances of the calcareous plankton (calcareous nannofossils) at time
440 of shale deposition, since this group is outcompeted by the diatoms when nutrients and Si supply to
441 the basin is high (Margaleff 1978, Balch 2004). The siliceous plankton blooms could then have
442 increased the organic carbon flux to the sea floor, thus supporting the abundant *Bolivina* spp. and
443 *Brizalina* spp. assemblages, known as characterising organic-rich bottom sediments and tolerating
444 dysoxic conditions (Barmawidjaja et al. 1992, Gooday 1988, Drinia et al. 2008, De Almeida et al.
445 2015). High runoff from the continent is also suggested by the high amount of shallow-water taxa
446 among benthic foraminifers, possibly reworked from shallower waters. All these evidences indicate
447 that lithologic and palaeobiological cycles at Moncalvo record climate cycles, likely correlated to
448 precession-driven insolation cycles, as already recorded in other Mediterranean sections (Blanc-
449 Valleron et al. 2002, Sierro et al. 2001, 2003, Krijgsman et al. 2002, Flores et al. 2005).
450 In the Banengo section the basic shale/marl pattern is interrupted by the occurrence of coarse-
451 grained beds and the lithologic cyclicity is not easily detected; however, the abundance fluctuation
452 of calcareous plankton taxa supports the hypothesis of climate control also in this section. In fact,
453 the relative abundances of *S. abies* are higher in the shales lower to zero in the marls. *Calcidiscus*
454 *leptoporus* (temperate, well mixed mesotrophic waters; Ziveri et al. 2004) shows an opposite, even
455 if less prominent, abundance fluctuation: it is absent in the shales, more abundant in the marls (up to
456 7% in cycle Bm1). Among planktonic foraminifers, abundance fluctuation of the cool-water
457 eutrophic taxa (*G. bulloides* and *G. falconensis, T. multiloba* and *T. quinqueloba*, *G. scitula* and *G.*
458 *suterae)* correlates with *Cd. leptoporus* abundances, confirming the climate control of the
459 shale/marl cycles. A comparable fluctuation of the calcareous plankton abundance has previously
460 been recorded in the Pollenzo section and has been linked to precession-driven climate cycles
461 (Violanti et al. 2013).
462 Following the above evidences from the Moncalvo and Banengo sections, the marly hemicycles,
463 deposited under cool/arid climate, were correlated to insolation minima (precession maxima),
464 whereas shaly hemicycles, deposited under warm/humid climate, were tied to insolation maxima

(precession minima). This is in agreement with previous works that recognized a precessional cyclicity in the Mediterranean Messinian sections on the basis of calcareous plankton abundance fluctuactions (Krijgsman et al. 2001, Flores et al. 2005, Riforgiato et al. 2008, among others). In the studied sections gypsum beds overlay a different number of shale/marl precessional cycle above the HCO of *T. multiloba* (Fig. 11). According to our data, the HCO of *T. multiloba* (recovered four cycles below the onset of the MSC in the Abad Composite; Sierro et al. 2001) occurs five cycles below the first gypsum bed in the Banengo section, similarly to what has already been recorded at Pollenzo, where gypsum occurs seven cycles above the HCO of *T. multiloba* (Dela Pierre et al. 2011, Violanti et al. 2013). This suggests that, in these sections, gypsum deposition was respectively delayed by ~21 ky and ~63 ky with respect to the Abad Composite section. In the two sections, the onset of the MSC is thus placed in Cycles Bm5 and Pm5. In the Moncalvo and Pollenzo sections the correlation to the Mediterranean reference sections is also based on the occurrence of the branching selenite facies in Cycles Mg4 and Pg3, that correlate to Cycle PLG6 (Dela Pierre et al. 2011). This also confirms that at Moncalvo the MSC onset should be placed in Cycle Mm3, suggesting that gypsum deposition is delayed by two precessional cycles (~42 ky) (Fig 11).

5.3. Bioevents at the onset of the MSC

In agreement with biostratigraphic and cyclostratigraphic data, the beginning of the MSC in the Banengo, Moncalvo and Pollenzo sections occurs in Cycles Bm5, Mm3 and Pm5, respectively. In the three sections a very remarkable sequence of bioevents characterizes the cycle recording the MSC onset, correlative to the first PLG cycle (Dela Pierre et al. 2011). These events are: the *S. abies* peak, followed or accompanied by peaks of *H. carteri*, *R. procera*, *U. rotula,* and *U. jafari*, the *G. scitula* and *G. suterae* influx, the disappearence of planktonic foraminifers >125 μm. These bioevents occur in the same stratigraphic order in all the three sections, are synchronous at the Piedmont Basin scale, and occur in the cycle deposited at the onset of the MSC and correlative to

491 cycle PLG1 at the Mediterranean scale (Fig. 11). In the Mediterranean reference sections no reliable
492 bioevents (other than the HCO of *T. multiloba*, four cycles below the onset) were used to
493 approximate the MSC onset, besides the decrease or complete absence of foraminifers, which was
494 regarded as a common and synchronous basin-wide event (Sprovieri et al. 1996, Bellanca et al.
495 2001, Blanc-Valleron et al. 2002, Manzi et al. 2007). In sections without distinct lithologic cyclicity
496 and/or lacking gypsum deposits (Fanantello section, Manzi et al. 2007; Legnagnone section,
497 Gennari et al. 2013) the absence of foraminifers was thus tentatively used as marker for the
498 beginning of the MSC. Neverthelss, in the last decade few studies demonstrated that calcareous
499 plankton does not disappear at time of gypsum deposition, both in sections where gypsum is
500 recorded (Wade and Bown 2006) and where the euxinic shale correlative to the first stage of the
501 MSC occur, such as in the Fanantello (Manzi et al. 2007) and in the Pollenzo (Violanti et al. 2013)
502 sections. In the latter section, as well as in the Banengo section, foraminifers in the fraction 63-125
503 μm continously occur above the onset of the MSC. Strikingly, in the Fanantello section the last
504 occurrence (LO) of foraminifers correlates to a very sharp *S. abies* peak; this level is regarded as
505 synchronous to the MSC onset due to direct correlation to the HO of foraminifers (Manzi et al.
506 2007); interestingly, calcareous nannofossils also occur above this level. Unpublished data (A.
507 Negri, pers. comm. 2016) confirm that in this section, where three *S. abies* abundance peaks were
508 recorded, the lowermost *S. abies* peak is followed by higher abundances of *H. carteri* and *U. rotula*
509 and correlates to the first PLG cycle.
510 Nearly monospecific calcareous nannofossil assemblages of *S. abies* have also been recorded
511 simultaneously with the HO of planktonic foraminifers in the pre-evaporitic sequence of the
512 Kalamaki section on Zakynthos Island in the Ionian Sea (Table S1; Karakitsios et al. 2016).
513 Further east, in the Pissouri section (Cyprus), unpublished data also show that the same sequence of
514 events (A. Negri, pers. comm. 2016) is recorded in a shale/marl cycle at the top of the section, just
515 below the gypsum. This gypsum overlays the shale/marl cycles of the Pakhna Fm. through an
516 erosional surface; this surface, recently interpreted as the Messinian Erosional Surface (Manzi et al.

517 2016), was overlooked in previous works (e.g. Krijgsman et al. 1999, Kouwenhoven et al. 2006,
518 Morigi et al. 2007). Furthermore, the upper part of the Pissouri section does not allow a
519 straightforward chronostratigraphic correlation since it lacks a clear magnetostratigraphic signal and
520 the HO *T. multiloba* has not been reported. Additionally, a slumped interval occurs in the top ten
521 metres of the section that could have been responsible for the erosion of one or more cycles. Owing
522 to these new observations, the age of the cycle recording the *S. abies* peak, previously dated at
523 5.999 Ma (Kouwenhoven et al. 2006), could be younger by 21 kyr (5.97 Ma) and be correlative of
524 the MSC onset.
525 Another section cropping out on Cyprus, the Tokhni section (Gennari et al. this volume), has been
526 recently studied by means of planktonic foraminifers and calcareous nannofossils; it records the
527 occurrence of high abundances of *H. carteri* and *U. rotula* four cycles above the HCO of *T.*
528 *multiloba*. Unfortunately in this cycle, the *S. abies* peak alone is not noticeable, since also the lower
529 cycles contain high abundance of this taxon in the shale beds. Nevertheless, the sequence of events
530 (*S. abies* peak, higher abundance of *H. carteri* and the oligotypic *U. rotula* assemblage), suggests
531 that this cycle is correlative to the first PLG cycle.
532 The sequence of calcareous plankton bioevents recorded in the Piedmont Basin and sychronous
533 with the onset of the MSC, could thus represent a reliable tool to identify this event at a
534 Mediterranean-wide scale.
535

536 **6. Conclusions**

537 In this work we address the biostratigraphic study of three sections straddling the MSC onset and
538 located in the Piedmont Basin (Banengo, Moncalvo and Pollenzo). Their correlation to the
539 Mediterranean reference sections from the Western, Central, and Eastern Mediterranean (Sierro et
540 al. 2001, Blanc-Valleron et al. 2002, Gennari et al. this volume) is based on the HCO of *T.*
541 *multiloba* and demonstrates that in Banengo, Moncalvo, and Pollenzo, gypsum deposition is

delayed by one, two and three precessional cycles with respect to the onset of the MSC, respectively.

In the Piedmont Basin the disappearance of calcareous plankton, previously suggested as a reliable event synchronous with the onset of the MSC, does not occur in the basal MSC cycle; calcareous nannofossils and foraminifers (both in the >125 μm and 63-125 μm size fractions) are recorded up to three cycles above the onset of the crisis.

In the basal MSC cycle a distinct sequence of bioevents (the prominent *S. abies* peak followed or accompanied by *H. carteri*, *R. procera*, and *Umbilicosphaera* spp. peaks, and the *G. scitula* and *G. suterae* influx), has been recorded. Among them, the *S. abies* and *U. rotula* peaks, also recorded in several Eastern Mediterranean sections, have a strong potential to become a reliable tool to recognize the onset of the MSC at a Mediterranean-Basin-wide scale, particularly in intermediate and deep water settings, where primary gypsum is not recorded.

To confirm the reliability of this sequence of bioevents, further work is needed on stratigraphic sections encompassing the onset of the Messinian salinity crisis, especially from the Western Mediterranean where detailed calcareous nannofossil data are still lacking. Moreover, the bioevents highlighted in this work can potentially provide a precise identification tool for the beginning of the MSC in deep-sea cores.

Acknowledgements

This research was funded by a MIUR (Ministero dell'Istruzione, dell'Università e della Ricerca, Italy) grant to M. Roveri (University of Parma, PRIN 2008) and by University of Torino funds to Dela Pierre (2013, 2014) and Violanti (2013). Many thanks are due to Maria Triantaphyllou, to an anonimous reviewer, and to the Editor Joerg Pross, whose constructive criticisms and suggestions greatly improved the original version of the manuscript.

References

568 Alve, E., Korsun, S., Schönfeld, J., Dijkstra, N., Golikova, E., Hess, S., Husum, K., Panieri, G.
569 2016. Foram-AMBI: A sensitivity index based on benthic foraminiferal faunas from the North-East
570 Atlantic and Arctic fjords, continental shelves and slopes. Marine Micropaleontology 122, 1-12.
571 Balch, W.M., 2004. Re-evaluation of the physiological ecology of coccolithophores. In: Thierstein,
572 H. R., Young, J. R. (Eds.), Coccolithophores-From molecular processes to global impact. Springer-
573 Verlag, Berlin, p. 165–190.
574 Barbieri, R., Panieri, G., 2004. How are benthic foraminiferal faunas influenced by cold seeps?
575 Evidence from the Miocene of Italy. Palaeogeography, Palaeoclimatology, Palaeoecology, 204,
576 257-275.
577 Barmawidjaja, D.M., Jorissen, F.J., Puskaric, S., Van der Zwaan, G.J., 1992. Microhabitat selection
578 by benthic foraminifera in the Northern Adriatic Sea. Journal of Foraminiferal Research 22 (4),
579 297-317.
580 Bè, A.W., Tolderlund, D.S., 1971. Distribution and ecology of living planktonic foraminifera in
581 surface waters of the Atlantic and Indian Oceans. In Funnell B.M. & Riedel W.R. (eds),
582 Micropaleontology of Oceans, Cambridge University Press, Cambridge. 105-149.
583 Bellanca, A., Caruso, A., Ferruzza, G., Neri, R., Rouchy, J.M., Sprovieri, M., Blanc-Valleron,
584 M.M., 2001. Transition from marine to hypersaline conditions in the Messinian Tripoli Formation
585 from the marginal areas of the central Sicilian Basin. Sedimentary Geology 140, 87-105.
586 Bergamin, L., Di Bella, L., Carboni, M.G., 1999. *Valvulineria bradyana (*Fornasini) in organic
587 matter-enriched environment (Ombrone River mouth, Central Italy). Il Quaternario. Italian Journal
588 of Quaternary Sciences 12 (1), 51-56.
589 Bernardi, E., 2013. Integrated stratigraphy of the Northernmost record of the Messinian salinity
590 crisis: new insights from the Tertiary Piedmont Basin. PhD thesis, University of Torino, Torino, p.
591 137.
592 Bigi, G., Cosentino, D., Parotto, M., Sartori, R., Scandone, P., 1990. Structural Model of Italy:
593 Geodinamic Project: Consiglio Nazionale delle Ricerche, S.EL.CA, scale 1:500 000, sheet 1.

Blanc-Valleron, M.M., Pierre, C., Caulet, J.P., Caruso, A., Rouchy, J.M., Cespuglio, G., Sprovieri, R., Pestrea, S., Di Stefano, E., 2002. Sedimentary, stable isotope and micropaleontological records of paleoceanographic change in the Messinian Tripoli Formation (Sicily, Italy). Palaeogeography, Palaeoclimatology, Palaeoecology 185, 255-286.

CIESM 2008. The Messinian Salinity Crisis from mega-deposits to microbiology - a consensus report. In: Briand, F. (Ed.), CIESM Workshop Monographs 33. 168 pp. Monaco.

Colom, G., 1974. Foraminiferos ibericos. Introducion al estudio de las especies bentonicas recientes. Investigacion Pesquera 38, (1), 1-245.

de Almeida, F. K., de Mello, R. M., Costa, K.B., Toledo, F.A.L., 2015. The response of deep-water benthic foraminiferal assemblages to changes in paleoproductivity during the Pleistocene (last 769.2 kyr), western South Atlantic Ocean. Palaeogeography, Palaeoclimatology, Palaeoecology 440, 201-212.

Dela Pierre, F., Bernardi, E., Cavagna, S., Clari, P., Gennari, R., Irace, A., Lozar, F., Lugli, S., Manzi, V., Natalicchio, M., Roveri, M., Violanti, D., 2011. The record of the Messinian salinity crisis in the Tertiary Piedmont Basin (NW Italy): The Alba section revisited. Palaeogeography, Palaeoclimatology, Palaeoecology 310, 238-255.

Dela Pierre, F., Clari, P., Bernardi, E., Natalicchio, M., Costa, E., Cavagna, S., Lozar, F., Lugli, S., Manzi, V., Roveri, M., Violanti, D., 2012. Messinian carbonate-rich beds of the Tertiary Piedmont Basin (NW Italy): Microbially-mediated products straddling the onset of the salinity crisis. Palaeogeography, Palaeoclimatology, Palaeoecology 344-345, 78-93.

Di Grande, A., Romeo, M., 1980. Caratteri lito-biostratigrafici dei depositi messiniani nell'area iblea (Sicilia sud-orientale). Rivista Italiana di Paleontologia e Stratigrafia 86, 855-916.

Diz, P. and Frances, G., 2008. Distribution of live benthic foraminifera in the Ría de Vigo (NW Spain). Marine Micropaleontology 66, 165-191.

618 D'Onofrio, S., Giannelli, L., Iaccarino, S., Morlotti, E., Romea, M., Salvatorini, G., Sampò, M.,
619 Sprovieri, R., 1975. Planktonic foraminifera from some Italian sections and the problem of the
620 lower boundary of the Messinian. Bollettino della Società Paleontologica Italiana 14, 177-196.
621 Drinia, H., Antonarakou, A., Kontakiotis, G., 2008. On the occurrence of Early Pliocene marine
622 deposits in the Ierapitrea Basin, Eastern Crete, Greece. Bullettin of Geosciences 83 (1), 63-78.
623 Flecker, R., Krijgsman, W., Capella, W., de Castro Martíns, C., Dmitrieva, E., Mayser, J.P.,
624 Marzocchi, A., Modestou, S., Ochoa, D., Simon, D., Tulbure, M., van den Berg, B., van der Schee,
625 M., de Lange, G., Ellam, R., Govers, R., Gutjahr, M., Hilgen, F., Kouwenhoven, T., Lofi, J., Meijer,
626 P., Sierro, F.J., Bachiri, N., Barhoun, N., Alami, A.C., Chacon, B., Flores, J.A., Gregory, J.,
627 Howard, J., Lunt, D., Ochoa, M., Pancost, R., Vincent, S., Yousfi, M.Z., 2015. Evolution of the
628 Late Miocene Mediterranean-Atlantic gateways and their impact on regional and global
629 environmental change. Earth-Science Reviews 150, 365–392.
630 Flores, J.A., Sierro, F.J., Filippelli, G.M., Barcena, M.A., Perez- Folgado, M., Vazquez, A., Utrilla,
631 R., 2005. Surface water dynamics and phytoplankton communities during deposition of cyclic late
632 Messinian sapropel sequences in the western Mediterranean. Marine Micropaleontology 56, 50-79.
633 Gennari, R., Manzi, V., Angeletti, L., Bertini, A., Biffi, U., Ceregato, A., Faranda, C., Gliozzi E.,
634 Lugli, S., Menichetti, E., Rosso, A., Roveri, M., Taviani, M., 2013. A shallow water record of the
635 onset of the Messinian salinity crisis in the Adriatic foredeep (Legnagnone section, Northern
636 Apennines). Palaeogeography, Palaeoclimatology, Palaeoecology 386, 145-164.
637 Gennari, R., Lozar, F., Turco, E., Dela Pierre, F., Manzi, V., Natalicchio, M., Lugli, S., Roveri, M.,
638 Schreiber B.C., Taviani, M., *this volume*. Integrated stratigraphy and paleoceanographic evolution
639 of the pre-evaporitic phase of the Messinian salinity crisis in the Eastern Mediterranean as recorded
640 in the Tokhni section (Cyprus island). DOI: 10.1127/nos/2017/0350
641 Gibbs, S., Shackleton, N., Young, J.R., 2004. Orbitally forced climate signals in mid-Pliocene
642 nannofossil assemblages. Marine Micropaleontology 51, 39-56.

643 Gooday, A.J., 1988. A response by benthic Foraminifera to the deposition of phytodetritus in the
644 deep-sea. Nature 332, 70-73.
645 Hammer, Ø., Harper, D.A.T., Ryan, P.D., 2008. PAST - PAlaeontological STatistics, ver. 1.77, 87
646 pp., http://folk.uio.no/ohammer/past.
647 Hemleben, C., Spindler, M., Anderson, O.R., 1989. Modern Planktonic Foraminifera. Springer-
648 Verlag, Berlin, 335 pp.
649 Hilgen, F.J., Krijgsman, W., 1999. Cyclostratigraphy and astrochronology of the Tripoli diatomite
650 formation (pre-evaporite Messinian, Sicily, Italy). Terra Nova 11, 16-22.
651 Iaccarino, S. 1985. Mediterranean Miocene and Pliocene planktic Foraminifera. In: Bolli, H.M.,
652 Saunders, J.B., Perch-Nielsen, K. (Eds.), Plankton Stratigraphy, Cambridge University Press,
653 Cambridge, p. 283-314.
654 Iaccarino, S.M., Bertini, A., Di Stefano, A., Ferraro, L., Gennari, R., Grossi, F., Lirer, F., Manzi, V.,
655 Menichetti, E., Ricci Lucchi, M., Taviani, M., Sturiale, G., Angeletti, L., 2008. The Trave section
656 (Monte dei Corvi, Ancona, Central Italy): an integrated paleontological study of the Messinian
657 deposits. Stratigraphy 5 (3-4), 281-306.
658 Karakitsios, V., Roveri, M., Lugli, S., Manzi, V., Gennari, R., Antonarakou, A., Triantaphyllou, M.,
659 Agiadi, K., Kontakiotis, G., Kafousia, N., De Rafelis, M., 2016. A record of the Messinian salinity
660 crisis in the eastern Ionian tectonically active domain (Greece, eastern Mediterranean). Basin
661 Research 28 (1), 1-31.
662 Kennett, J.P., Srinivasan, M.S., 1983. Neogene Planktonic Foraminifera - A phylogenetic atlas.
663 Hutchinson Ross Publishing Company, Stroudsburg, Pennsylvania, U.S.A. 265 pp.
664 Kouwenhoven, T.J., Seidenkrantz, M.-S., Van der Zwaan, G.J., 1999. Deep-water changes: The
665 near-synchronous disappearance of a group of benthic foraminifera from the late Miocene
666 Mediterranean. Palaeogeography, Palaeoclimatology, Palaeoecology 152, 259-281.

667 Kouwenhoven, T.J., Morigi, C., Negri, A., Giunta, S., Krijgsman, W., Rouchy, J.M., 2006.
668 Paleoenvironmental evolution of the eastern Mediterranean during the Messinian: Constraints from
669 integrated microfossil data of the Pissouri Basin (Cyprus). Marine Micropaleontology 60, 17-44.
670 Krijgsman, W., Hilgen, F.J., Raffi, I., Sierro, F.J., Wilson, D.S., 1999. Chronology, causes and
671 progression of the Messinian salinity crises. Nature 400, 652-655.
672 Krijgsman, W., Hilgen, F.J., Fortuin, A., Sierro, F.J., 2001. Astrochronology for the Messinian
673 Sorbas Basin (SE Spain) and orbital (precessional) forcing for evaporate cyclicity. Sedimentary
674 Geology 140, 43–60.
675 Krijgsman, W., Blanc-Valleron, M.M., Flecker, R., Hilgen, F.J., Kouwenhoven, T.J., Merle, D.,
676 Orzsag-Sperber, F., Rouchy, J.M., 2002. The onset of the Messinian salinity crisis in the Eastern
677 Mediterranean (Pissouri Basin, Cyprus). Earth and Planetary Science Letters 194 (3-4), 299-310.
678 Laskar, J., Robutel, P., Joutel, F., Gastineau, M., Correia, A.C.M., Levrard, B., 2004. A long-term
679 numerical solution for the insolation quantities of the Earth. Astronomy and Astrophysics 428, 261-
680 285.
681 Loeblich, A.R., Tappan, H. 1988. Foraminiferal genera and their classification. Van Nostrand
682 Reinhold, New York, U.S.A. pp. 1-970, pls. 1-847.
683 Lourens, L.J., Hilgen, F.J., Shackleton, N.J., Laskar, J., Wilson, D., 2004. The Neogene Period. In:
684 Gradstein, F., Ogg, J., Smith, A. (Eds), A Geologic Time Scale 2004, Cambridge University Press,
685 Cambridge, pp. 409-440.
686 Lozar, F., Violanti, D., Dela Pierre, F., Bernardi, E., Cavagna, S., Clari, P., Irace, A., Martinetto, E.,
687 Trenkwalder, S., 2010. Calcareous nannofossils and foraminifers herald the Messinian salinity
688 crisis: the Pollenzo section (Alba, Cuneo; NW Italy). Géobios 43, 21-32.
689 Lugli, S., Manzi, V., Roveri, M., Schreiber, B.C., 2010. The Primary Lower Gypsum in the
690 Mediterranean: a new facies interpretation for the first stage of the Messinian salinity crisis.
691 Palaeogeography, Palaeoclimatology, Palaeoecology 297, 83-99.

692 Manzi, V., Lugli, S., Ricci Lucchi, F., Roveri, M., 2005. Deep-water clastic evaporites deposition in
693 the Messinian Adriatic foredeep (northern Apennines, Italy): did the Mediterranean ever dry out?
694 Sedimentology 52, 875-902.
695 Manzi, V., Roveri, M., Gennari, R., Bertini, A., Biffi, U., Giunta, S., Iaccarino, S.M., Lanci, L.,
696 Lugli, S., Negri, A., Riva, A., Rossi, M.E., Taviani, M., 2007. The deep-water counterpart of the
697 Messinian Lower Evaporites in the Apennine foredeep: The Fanantello section (Northern
698 Apennines, Italy). Palaeogeography, Palaeoclimatology, Palaeoecology 251, 470-499.
699 Manzi, V., Gennari, R., Hilgen, F., Krijgsman, W., Lugli, S., Roveri, M., Sierro, F.J., 2013. Age
700 refinement of the Messinian salinity crisis onset in the Mediterranean. Terra Nova 25, 315-322.
701 Manzi, V., Lugli, S., Roveri, M., Dela Pierre, F., Gennari, R., Lozar, F., Natalicchio, M., Schreiber,
702 B.C., Taviani, M., Turco, E., 2016. The Messinian salinity crisis in Cyprus: a further step towards a
703 new stratigraphic framework for Eastern Mediterranean. Basin Research 28, 207-236.
704 Margalef, R., 1978. Life-forms of phytoplankton as survival alternatives in an unstable
705 environment. Oceanologica Acta 1, 493-509.
706 Milker, Y, Schmiedl, G., 2012. A taxonomic guide to modern benthic shelf foraminifera of the
707 western Mediterranean Sea. Palaeontologia Electronica, 15 (2), 1-134.
708 Morigi, C., Negri, A., Giunta, S., Kouwenhoven, T., Krijgsman, W., Blanc-Valleron, M.M.,
709 Orszag-Sperber, F., Rouchy, J.-M., 2007. Integrated quantitative biostratigraphy of the latest
710 Tortonian-early Messinian Pissouri section (Cyprus): An evaluation of calcareous plankton
711 bioevents. Géobios 40, 267-279.
712 Murray, J.W., 2006. Ecology and Applications of Benthic Foraminifera. Cambridge University
713 Press. Cambridge. 426 p.
714 Orszag-Sperber, F., Caruso, A., Blanc-Valleron, M.-M., Merle, D., Rouchy, J.M., 2009. The onset
715 of the Messinian salinity crisis: insights from Cyprus sections. Sedimentary Geology 217, 52-64.
716 Perch-Nielsen, K., 1985. Cenozoic calcareous nannofossils. In: Bolli, H.M., Saunders, J.B., Perch-
717 Nielsen, K. (Eds.), Plankton Stratigraphy. Cambridge University Press, Cambridge, pp. 427-554.

718 Pujol, C., Vergnaud Grazzini, C., 1995. Distribution patterns of live planktic foraminifers as related
719 to regional hydrography and productive systems of the Mediterranean Sea. Marine
720 Micropaleontology 25, 187-217.
721 Pujos, A., 1987. Late Eocene to Pleistocene Medium-Sized and Small-Sized "Reticulofenestrids"
722 Abhandlungen der Geologischen Bundesanstalt 39, 239-277.
723 Raffi, I., Mozzato, C.A., Fornaciari, E., Hilgen, F.J., Rio, D., 2003. Late Miocene calcareous
724 nannofossil biostratigraphy and astrobiochronology for the Mediterranean region.
725 Micropaleontology 49, 1-26.
726 Riforgiato, F., Foresi, L.M., Aldinucci, M., Mazzei, R., Donia, F., Gennari, R., Salvatorini, G.,
727 Sandrelli, F., 2008. Foraminiferal record and astronomical cycles: An example from the Messinian
728 pre-evaporitic Gello Composite Section (Tuscany, Italy). Stratigraphy, 5 (3-4), 265-280.
729 Roveri, M., Manzi, V., Ricci Lucchi, F., Rogledi, S., 2003. Sedimentary and tectonic evolution of
730 the Vena del Gesso Basin (Northern Apennines, Italy): implications for the onset of the Messinian
731 salinity crisis. Geological Society of America Bulletin 115, 387-405.
732 Roveri, M., Bertini, A., Cosentino, D., Di Stefano, A., Gennari R., Gliozzi, E., Grossi, F., Iaccarino
733 S.M., Lugli, S., Manzi, V., Taviani, M., 2008. A high-resolution stratigraphic framework for the
734 latest Messinian events in the Mediterranean area. Stratigraphy 5, 322-342.
735 Roveri, M., Flecker, R., Krijgsman, W., Lofi, J., Lugli, S., Manzi, V., Sierro, F.J., Bertini, A.,
736 Camerlenghi, A., de Lange, G.J., Govers, R., Hilgen, F.J., Hübscher, C., Meijer, P.T., Stoica, M.,
737 2014. The Messinian Salinity Crisis: past and future of a great challenge for marine sciences.
738 Marine Geology 352, 25-58.
739 Serrano, F., Gonzales-Donoso, J.M., Linares, D., 1999. Biostratigraphy and paleoceanography of
740 the Pliocene at Site 975 (Menorca rise) and 976 (Alboran Sea) from a quantitative analysis of the
741 planktonic foraminiferal assemblages. In: Zahn, R., Comas, M.C., Klaus, A., (Eds.), ODP Science
742 Results 161, 185-195.

743 Sgarrella, F., Moncharmont, Zei M., 1993. Benthic foraminifera of the Gulf of Naples (Italy):
744 systematics and autoecology. Bollettino della Società Paleontologica Italiana 32 (2), 145-264.
745 Sierro, F.J., Hilgen, F.J., Krijgsman, W., Flores, J.A., 2001. The Abad composite (SE Spain): a
746 Mediterranean and global reference section for the Messinian. Palaeogeography, Palaeoclimatology,
747 Palaeoecology 168, 141-169.
748 Sierro, F.J., Flores, J.A., Bárcena, M.A., Vázquez, A., Utrilla, R., Zamarreño, Y., 2003. Orbitally-
749 controlled oscillations in the planktonic communities and cyclical changes in the western
750 Mediterranean hydrography during the Messinian. Palaeogeography, Palaeoclimatology,
751 Palaeoecology 190, 289-316.
752 Sprovieri, R., Di Stefano, E., Caruso, A., Bonomo, S., 1996. High resolution stratigraphy in the
753 Messinian Tripoli Formation in Sicily. Palaeopelagos 6, 415-435.
754 Suc, J.-P., Violanti, D., Londeix, L., Poumot, C., Robert, C., Clauzon, G., Gautier, F., Turon, J-L.,
755 Ferrier, J., Chikhi, H., Cambon, G., 1995. Evolution of the Messinian Mediterranean environments:
756 the Tripoli Formation at Capodarso (Sicily, Italy). Review of Palaeobotany and Palynology 87, 51-
757 79.
758 Van Hinsbergen, D.J.J., Kouwenhoven, T.J., Van der Zwaan, G.J., 2005. Paleobathymetry in the
759 backstripping procedure: Correction for oxygenation effects on depth estimates. Palaeogeography,
760 Palaeoclimatology, Palaeoecology 221, 245-265.
761 Van Morkhoven, F.P.C.M., Berggren, W.A., Edwards, A.S., 1986. Cenozoic cosmopolitan deep-
762 water benthic foraminifera. Bulletin des centres de recherches exploration-production Elf-Aquitaine
763 11, 1-421.
764 Violanti, D. 1996. Taxonomy and distribution of *Bulimina echinata* and relations with the Messinian
765 paleoenvironment. Bollettino della Società Paleontologica Italiana, Spec. Vol. 3, 243-253.
766 Violanti, D., Lozar, F., Dela Pierre, F., Natalicchio, M., Bernardi, E., Clari, P., Cavagna, S., 2013.
767 Stress tolerant microfossils of a Messinian succession from the northern Mediterranean basin

768 (Pollenzo section, Piedmont, Northwestern Italy). Bollettino della Società Paleontologica Italiana
769 52 (1), 45-54.
770 Violanti, D., Trenkwalder, S., Lozar, F., Gallo, L.M., 2009. Micropalaeontological analyses of the
771 Narzole core: biostratigraphy and palaeoenvironment of the late Messinian and early Zanclean of
772 Piedmont (Northwestern Italy). Bollettino della Società Paleontologica Italiana 48, 167-181.
773 Wade, B.S., Bown, P.R., 2006. Calcareous nannofossils in extreme environment: the Messinian
774 Salinity Crisis, Polemi Basin, Cyprus. Palaeogeography, Palaeoclimatology, Palaeoecology 233,
775 271-286.
776 Wright, R., 1978. Neogene paleobathymetry of the Mediterranean based on benthic foraminifers
777 from DSDP Leg 42A. In K.J. Hsu, L. Montadert et al., Initial Reports DSDP, 42A, 837-844.
778 Ziveri, P., Rutten, A., de Lange, G.J., Thomson, J., Corselli, C., 2000. Present day coccolith fluxes
779 recorded in central eastern Mediterranean sediment traps and surface sediments. Palaeogeography
780 Palaeoclimatology Palaeoecology 158, 175–195.
781 Ziveri, P., Baumann, K.-H., Böckel, B., Bollmann, J., Young, J.R., 2004. Present day
782 coccolithophore biogeography of the Atlantic Ocean. In: Thierstein, H.R., Young, J.R. (Eds.),
783 Coccolithophores: From Molecular Processes to Global Impact. Springer Verlag, pp. 529–562.
784

785 Figure captions

786 Fig. 1. A) Structural sketch of NW Italy (modified from Bigi et al. 1990). AM: Alto Monferrato;
787 BG: Borbera-Grue; MO: Monferrato; TH: Torino Hill; VVL: Villalvernia–Varzi line; PTF: Padane
788 Thrust Front; SVZ: Sestri-Voltaggio zone. Circled numbers correspond to location of the studied
789 sections: 1) Banengo; 2) Moncalvo; 3) Pollenzo. B) Schematic cross section (SW to NE), flattened
790 at the base of the Pliocene, showing the relationships among the Messinian units (modified from
791 Dela Pierre et al. 2011). Not to scale. PLG: Primary Lower Gypsum; RLG: Resedimented Lower

792 Gypsum; CRB: carbonate-rich beds; SKB: Sturani key-bed; MES: Messinian erosional surface.
793 Numbers of the three studied sections as in fig 1A.
794 Fig. 2. Banengo section: Chronostratigraphy, calcareous plankton biostratigraphy, lithostratigraphy,
795 sample location, percentage variation of the main calcareous nannofossil taxa. PLG: Primary Lower
796 Gypsum. Cycles Bg2 to Bg4 are not shown.
797 Fig. 3. Banengo section: Chronostratigraphy, calcareous plankton biostratigraphy, lithostratigraphy,
798 sample location, percentage variations of the P/(P+B) ratio, the main planktonic foraminiferal taxa,
799 warm-water oligotrophic indicators, and cool-water eutrophic indicators. Grey bands highlight
800 samples where the counting of the >125 μm fraction was not possible; see text for details. Legend
801 as in Fig. 2.
802 Fig. 4. Banengo section: Chronostratigraphy, calcareous plankton biostratigraphy, lithostratigraphy,
803 sample location, percentage variation of the main benthic foraminiferal taxa of DO/B = Deep Outer
804 neritic to Bathyial taxa, and of SW= Shallow Water taxa. SH: Shannon Index (H). Legend as in Fig.
805 2.
806 Fig. 5. Moncalvo section: Chronostratigraphy, calcareous plankton biostratigraphy,
807 lithostratigraphy, sample location, percentage variation of the main calcareous nannofossil taxa;
808 $CaCO_3$ percentage is also shown, together with qualitative abundance of diatoms (N: none; R: rare;
809 F: few; C: common; A: abundant; VA: very abundant). Cycles Mg2 to Mg5 are not shown. Legend
810 as in Fig. 2.
811 Fig. 6. Moncalvo section: Chronostratigraphy, calcareous plankton biostratigraphy,
812 lithostratigraphy, sample location, percentage variation of the P/(P+B) ratio, of the main planktonic
813 foraminiferal taxa, of W/O = Warm-water Oligotrophic indicators, and of C/E = Cool-water
814 Eutrophic indicators. Grey bands highlight samples where the counting of the >125 μm fraction was
815 not possible; see text for details. Legend as in Fig. 2 and 5.
816 Fig. 7. Moncalvo section: Chronostratigraphy, calcareous plankton biostratigraphy,
817 lithostratigraphy, sample location, percentage variation of the main benthic foraminiferal taxa, and

818 of DO/B = Deep Outer neritic to Bathyal taxa, and of SW = Shallow Water taxa. SH: Shannon
819 Index (H). Legend as in Fig. 2 and 5.
820 Fig. 8. Pollenzo section: Chronostratigraphy, calcareous plankton biostratigraphy, lithostratigraphy,
821 sample location, percentage variation of the main calcareous nannofossil taxa (modified from
822 Violanti et al. 2013).
823 Fig. 9. Pollenzo section: Chronostratigraphy, calcareous plankton biostratigraphy, lithostratigraphy,
824 sample location, percentage variation of the P/(P+B) ratio, of the main planktonic foraminiferal taxa
825 (modified from Violanti et al. 2013), of W/O = Warm-water Oligotrophic indicators, and of C/E =
826 Cool-water Eutrophic indicators. Legend as in Fig. 8.
827 Fig. 10. Pollenzo section: Chronostratigraphy, calcareous plankton biostratigraphy,
828 lithostratigraphy, sample location, percentage variation of the main benthic foraminiferal taxa
829 (modified from Violanti et al., 2013) and of DO/B = Deep Outer neritic to Bathyal taxa, and of SW
830 = Shallow Water taxa. SH: Shannon Index (H). Legend as in Fig. 8.
831 Fig. 11. Bed by bed correlation of the three studied sections (simplified and not to scale) to the PLG
832 cycles of the first stage of the MSC (as recorded in the Perales section, modified from Manzi et al.
833 2013) and to the Summer insolation 65°N (Laskar et al. 2004). Bioevent at the Mediterranean scale:
834 18a: HCO of *T. multiloba* (number as in Gennari et al. this volume). Local event; A: last *Orbulina*
835 spp. peak. The insert shows the bioevents proposed for the identification of the MSC onset. LR 125
836 PF: Last Recovery of planktonic foraminifers >125 μm.
837
838 Appendix 1 – List of deep outer neritic/bathyal foraminiferal taxa counted in the studied sections. b
839 = Banengo, m = Moncalvo, p = Pollenzo
840 Appendix 2 - List of shallow-water foraminiferal taxa counted in the studied sections. b = Banengo,
841 m = Moncalvo, p = Pollenzo

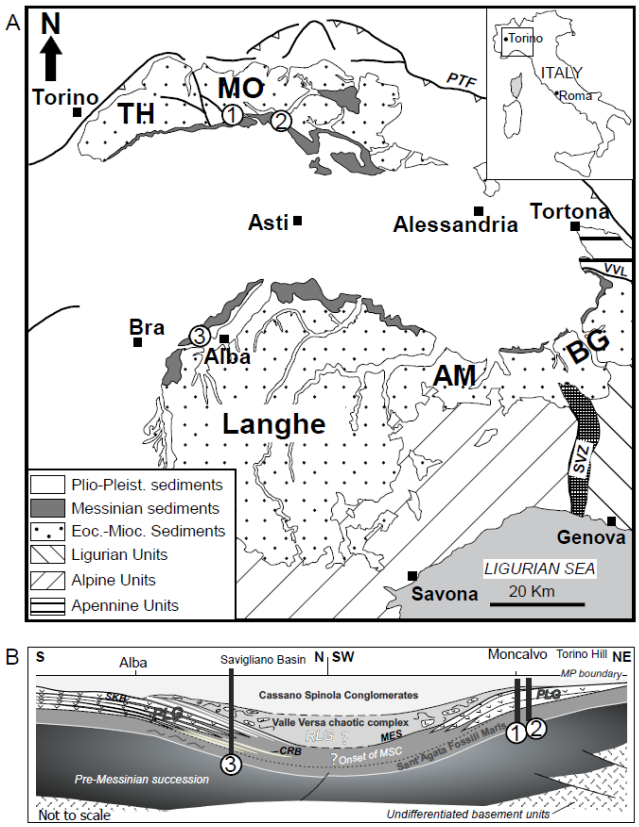

Lozar et al. Fig. 1

842

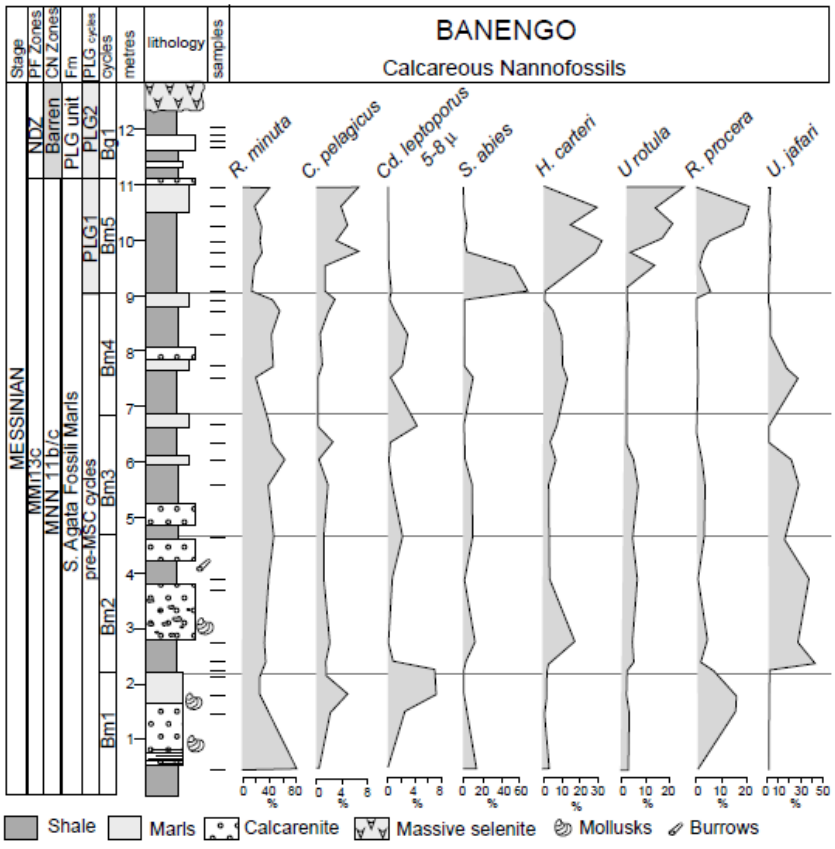

Lozar et al. Fig. 2

843

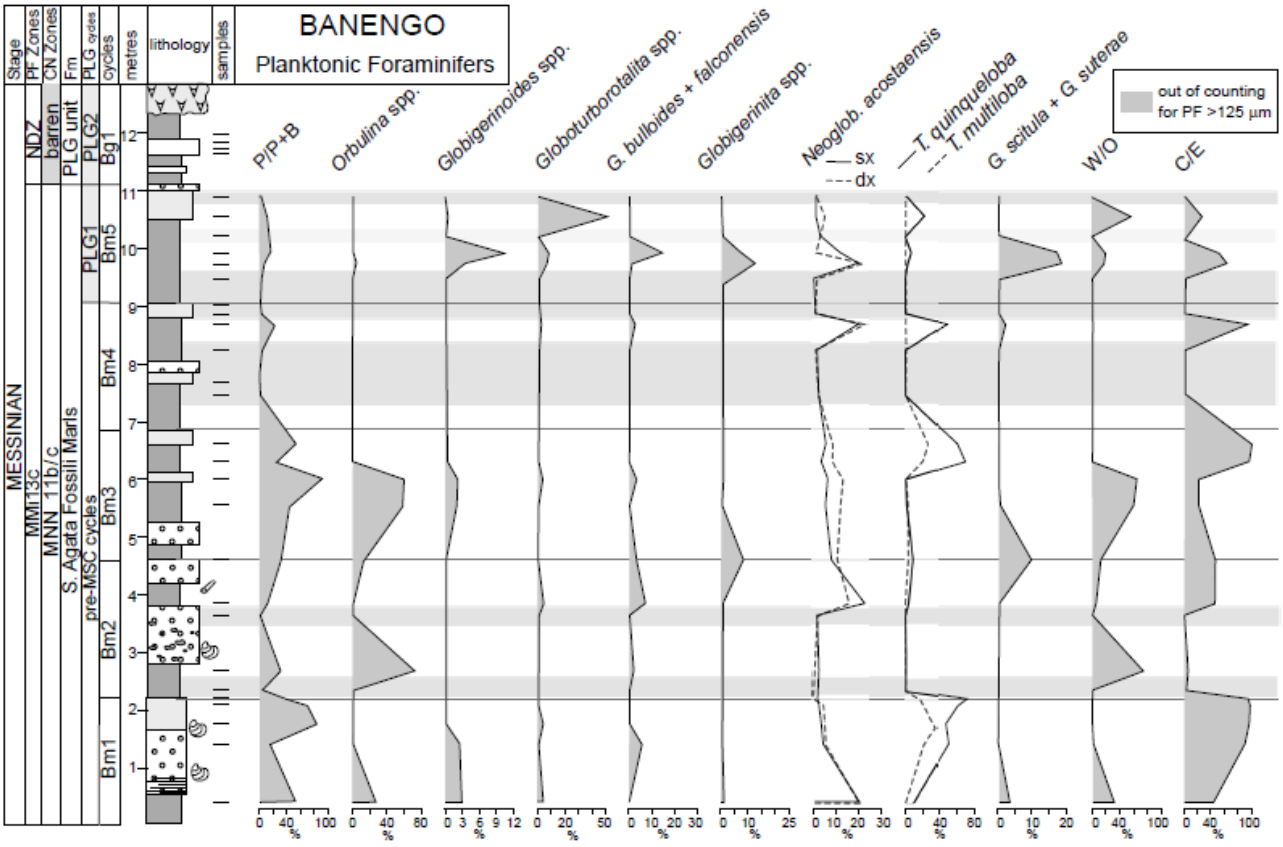

844

Lozar et al. Fig. 3

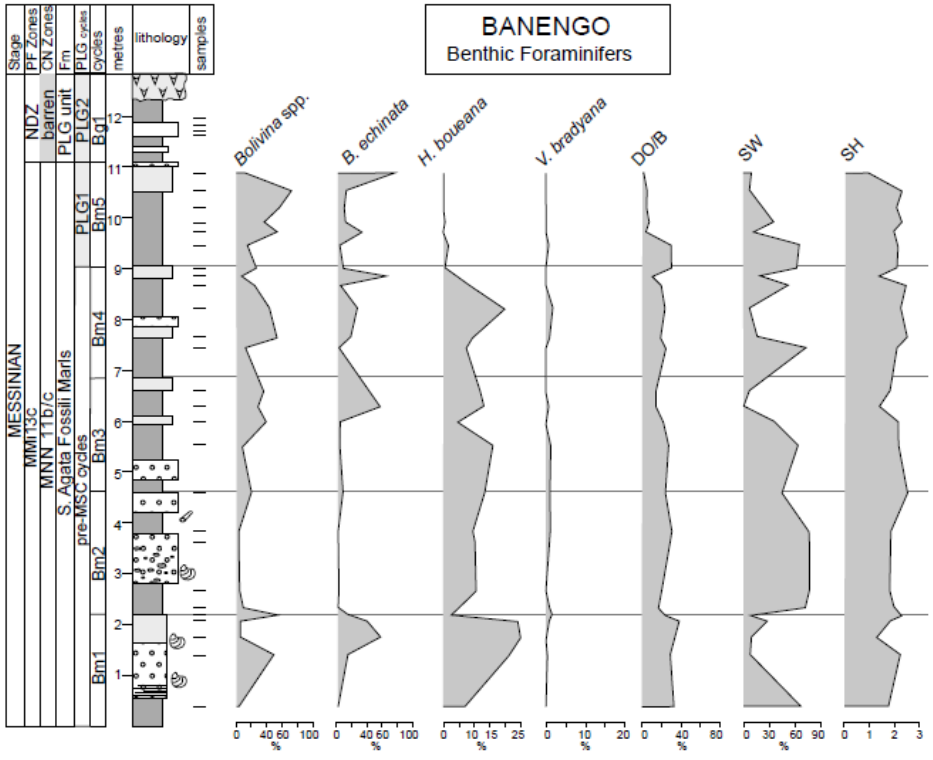

845

Lozar et al. Fig. 4

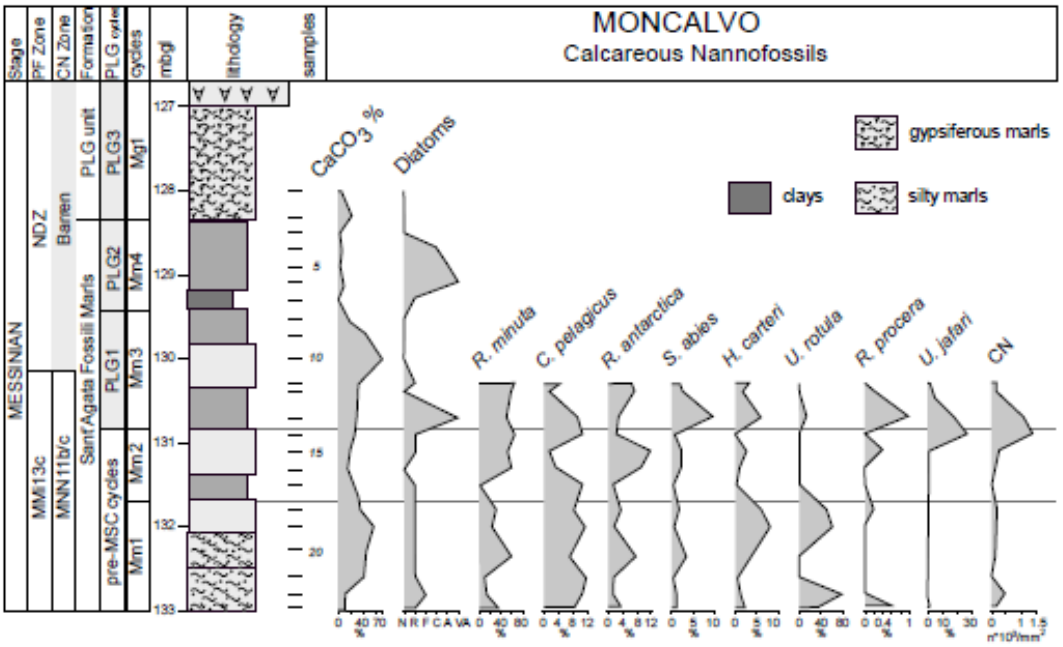

Lozar et al. Fig. 5

846

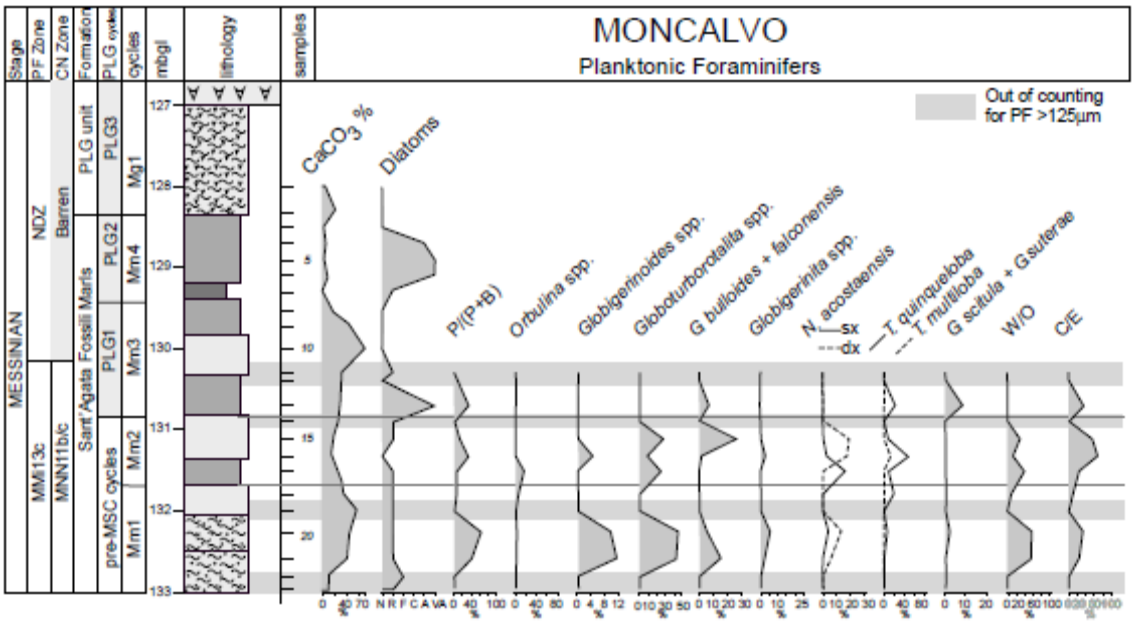

Lozar et al. Fig. 6

847

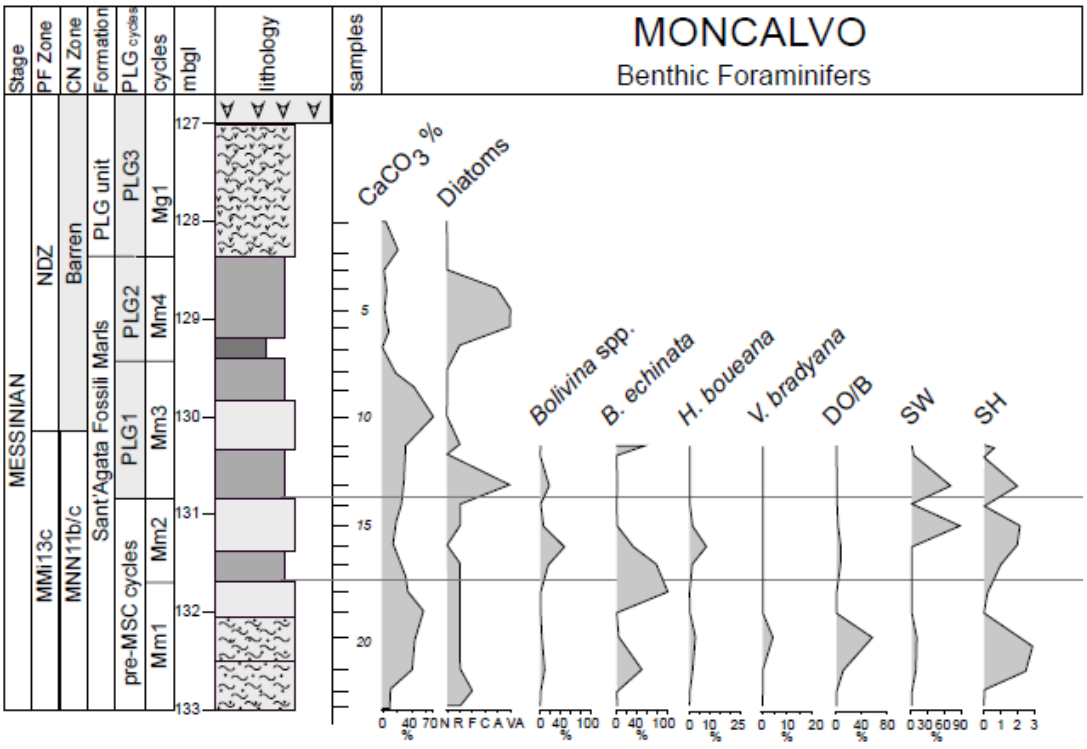

848

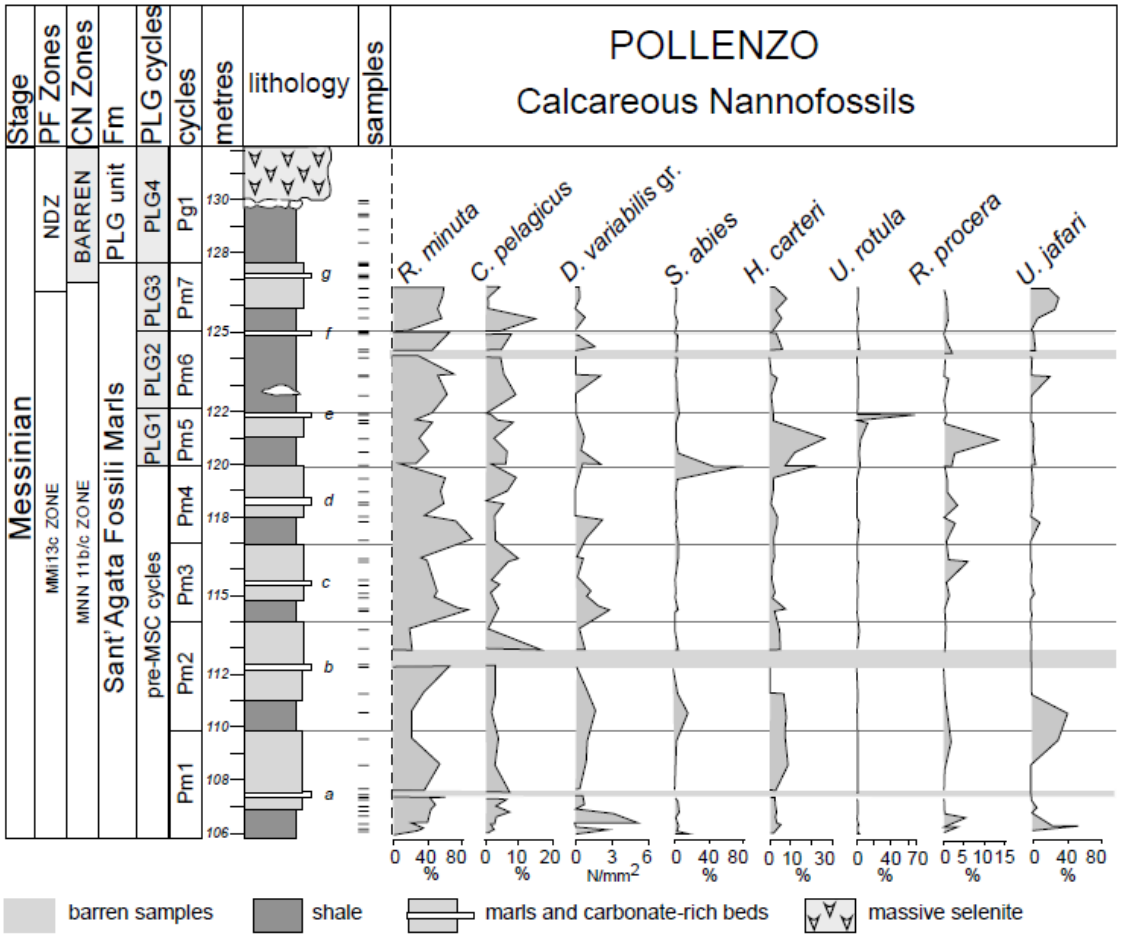

Lozar et al., fig 8

849

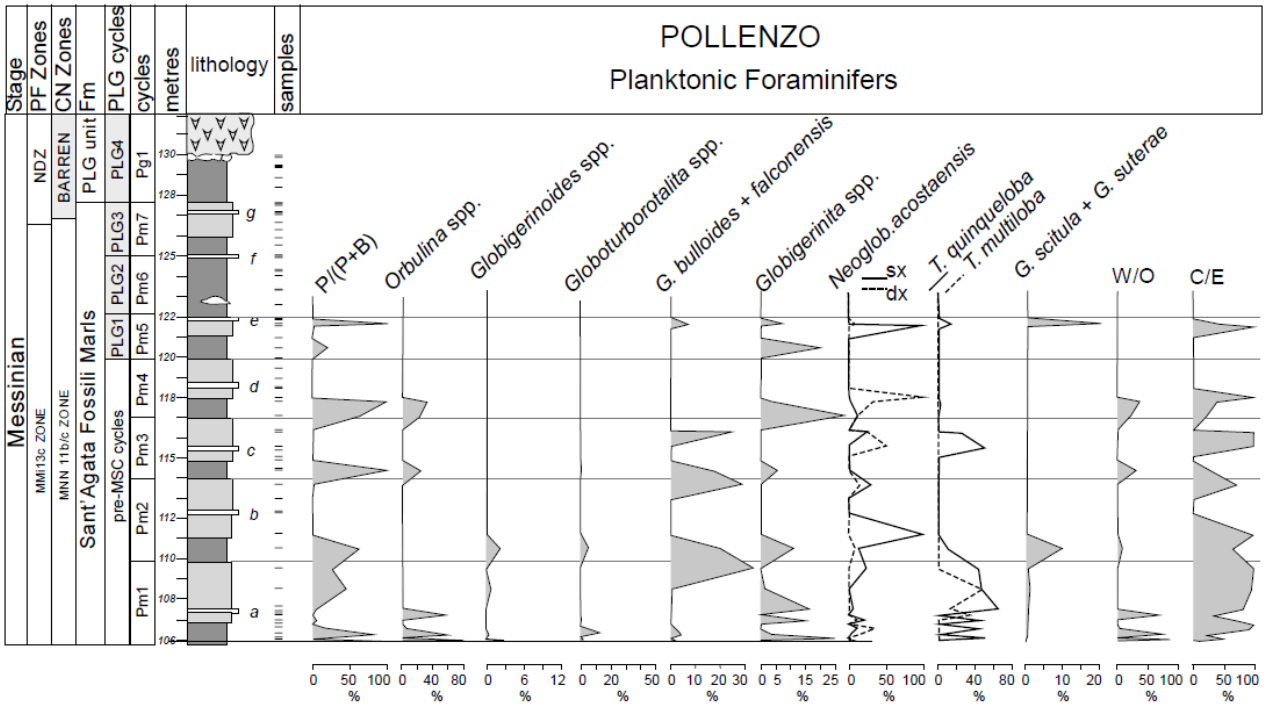

Lozar et al. fig 9

850

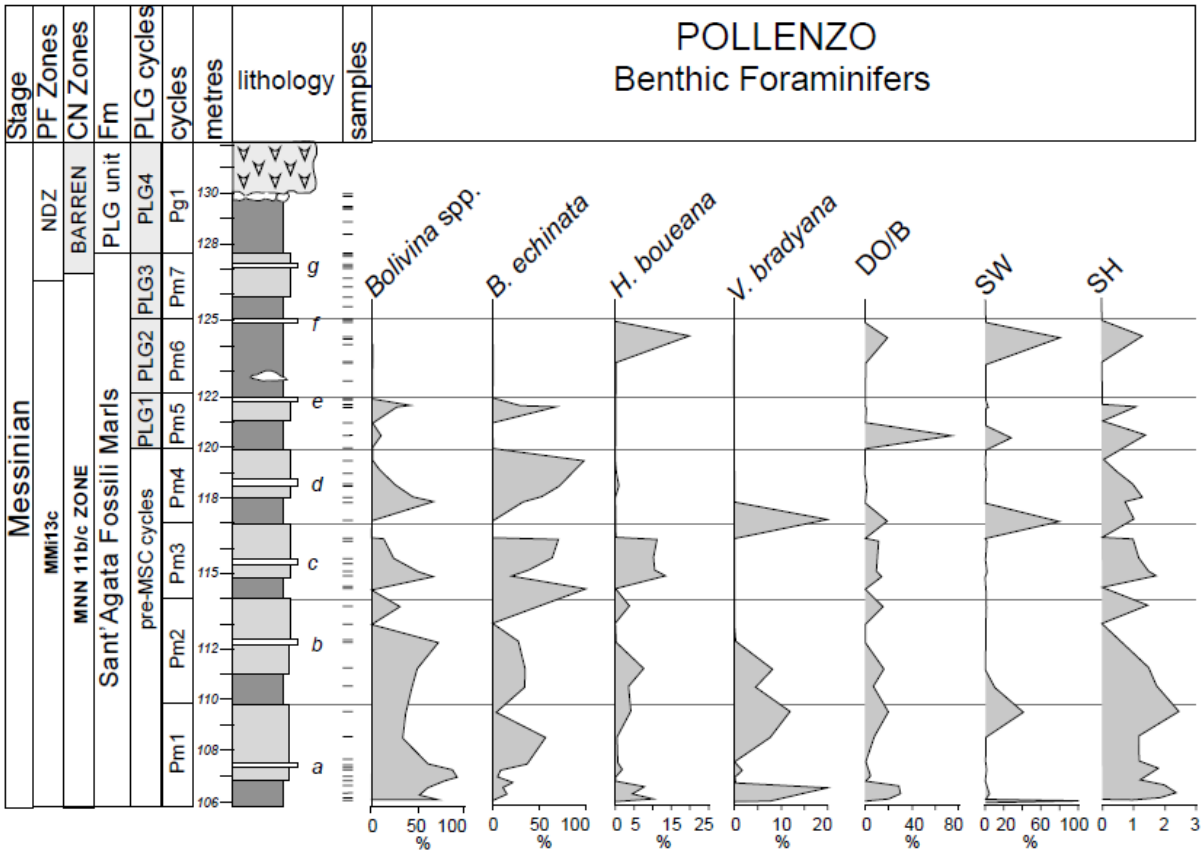

Lozar et al. Fig 10

851

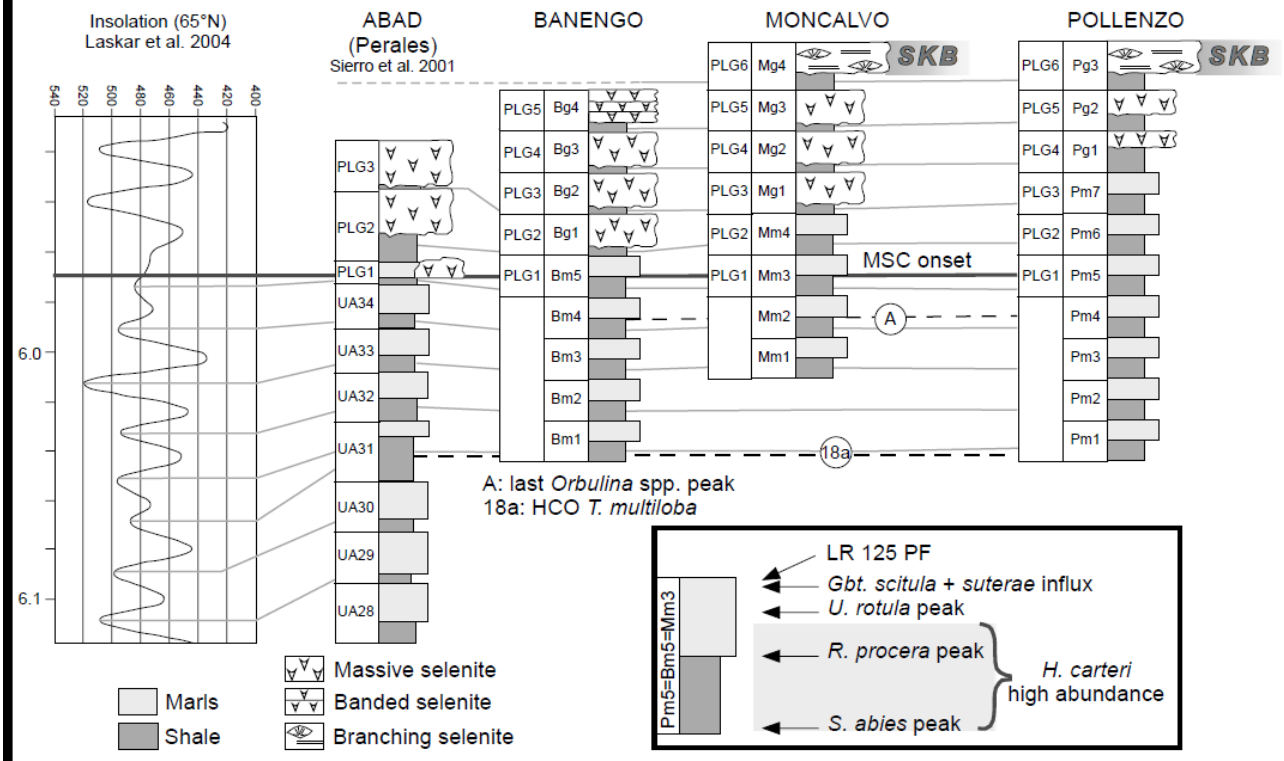

Lozar et al. Fig. 11

852